AD_____

Award Number: DAMD17-99-1-9294

TITLE: Automated Spot Mammography for Improved Imaging of Dense Breasts

PRINCIPAL INVESTIGATOR: Mitchell M. Goodsitt, Ph.D.

CONTRACTING ORGANIZATION: University of Michigan
Ann Arbor, Michigan 48109-1274

REPORT DATE: October 2002

TYPE OF REPORT: Annual

PREPARED FOR: U.S. Army Medical Research and Materiel Command
Fort Detrick, Maryland 21702-5012

DISTRIBUTION STATEMENT: Approved for Public Release;
Distribution Unlimited

The views, opinions and/or findings contained in this report are those of the author(s) and should not be construed as an official Department of the Army position, policy or decision unless so designated by other documentation.

REPORT DOCUMENTATION PAGE

Form Approved
OMB No. 074-0188

1. AGENCY USE ONLY (Leave blank)	2. REPORT DATE	3. REPORT TYPE AND DATES COVERED
	October 2002	Annual (15 Sep 01 - 14 Sep 02)

4. TITLE AND SUBTITLE
Automated Spot Mammography for Improved Imaging of Dense Breasts

5. FUNDING NUMBERS
DAMD17-99-1-9294

6. AUTHOR(S)
Mitchell M. Goodsitt, Ph.D.

7. PERFORMING ORGANIZATION NAME(S) AND ADDRESS(ES)

University of Michigan
Ann Arbor, Michigan 48109-1274

E-Mail: goodsitt@umich.edu

8. PERFORMING ORGANIZATION REPORT NUMBER

9. SPONSORING / MONITORING AGENCY NAME(S) AND ADDRESS(ES)

U.S. Army Medical Research and Materiel Command
Fort Detrick, Maryland 21702-5012

10. SPONSORING / MONITORING AGENCY REPORT NUMBER

11. SUPPLEMENTARY NOTES

Report contains color.

12a. DISTRIBUTION / AVAILABILITY STATEMENT

Approved for Public Release; Distribution Unlimited

12b. DISTRIBUTION CODE

13. ABSTRACT *(Maximum 200 Words)*

We are developing an automated stereo spot mammography technique to improve imaging of lesions within dense breast tissue.

During the third year of this project, our work was devoted primarily to developing: 1) software for an improved observer study to compare regions in mammograms that are selected by radiologists and the computer for spot imaging, and 2) software and hardware to implement the automated spot collimation component of the auto stereo spot technique. Based on radiologists' evaluations of the software used in our observer study performed during the second year of this project, we wrote new algorithms to display digitized mammograms at 200 μm and 400 μm resolution, which are 4 and 2 x better resolution than the 800 μm resolution employed previously. The new programs also allowed the radiologists to trace regions for spot imaging at either or both of these resolutions. In addition, we applied our CAD group's analysis techniques to the images so we could compare the regions selected by the computer with those selected by the radiologists. The spot collimation hardware was built and software was written to select spot regions and automatically move the collimator blades to restrict the x-ray beam to those regions. A phantom study was performed to verify proper auto-spot collimation.

14. SUBJECT TERMS	15. NUMBER OF PAGES
breast cancer, software, hardware, CAD group analysis technique	37
	16. PRICE CODE

17. SECURITY CLASSIFICATION OF REPORT	18. SECURITY CLASSIFICATION OF THIS PAGE	19. SECURITY CLASSIFICATION OF ABSTRACT	20. LIMITATION OF ABSTRACT
Unclassified	Unclassified	Unclassified	Unlimited

(3) TABLE OF CONTENTS

(4) INTRODUCTION

The purpose of our project is to develop a novel technique for improved imaging of suspicious dense regions within full-field digital mammograms. The basic idea is to automatically detect any large dense region within a whole breast digital mammogram, and to take a second 3D stereo digital mammogram of only that region using automated spot collimation, manual x-ray tube shift for the left- and right-eye stereo images, and stereoscopic viewing of the images on a stereo display system. This second "stereo spot mammogram" is taken within seconds of the full-field mammogram while the breast is maintained in the same compression. Since only the dense region is exposed, detector saturation will not be an issue. Restriction of the x-ray beam to a small area will limit the amount of breast tissue exposed to radiation with the technique and will decrease the volume of tissue that scatters x-rays thereby improving the contrast between a lesion and its surrounding dense breast tissue. Stereoscopic image acquisition and display will enable radiologists to view the suspicious regions in 3-D. This will reduce the tissue superposition problem inherent in conventional single projection mammography, whereby lesions can sometimes be camouflaged by overlying and/or underlying tissues, and normal tissues can sometimes overlap producing an object in the image with a lesion-like appearance. Furthermore, in comparison with conventional spot compression, the automated technique should produce more accurate spot imaging of suspicious regions because it eliminates the need for the repositioning of the breast between the full-field and spot images, and the "spot" location is determined by computer analysis of the digital full-breast image rather than estimated by eye from a radiograph. In brief, the project entails development of software to analyze digital mammograms and automatically delineate suspicious dense tissue regions, and the development of hardware to automatically collimate the x-ray beam to those regions and to enable stereo spot imaging of those regions while maintaining the breast in the same position and compression as for the original full-breast digital mammogram.

(5) BODY

We applied and received approval for a 1 year no cost time extension for our project to assure adequate completion of all of the tasks in our Modified Statement of Work (dated January 7,2002). Therefore the following is a third year rather than a final report. During the third year of this project (September 15, 2001 - September 14, 2002), the following was accomplished relative to the tasks in the approved modified statement of work.

A) Task 1: Develop software to recognize and delineate dense breast regions in full-breast mammograms.

Last year, we described the further development of a computer program that allowed radiologists to trace up to 3 regions for spot imaging in digitized mammograms and preliminary results of an observer study that was performed to compare the regions selected by the radiologists. This year, we developed more sophisticated analysis tools to compare the regions selected by the radiologists and reported on the results at the American Association of Physicists in Medicine (AAPM) Meeting in Montreal, Canada, July 14-18, 2002.[1] The analysis tools automatically ordered the ratios of the intersection divided by union areas of the regions selected by each combination of 4 radiologists taken two at a time and computed mean standard deviation, minimum, maximum statistics of the ratios for 177 digitized mammograms. The same analysis tools were also applied to regions selected by 2 radiologists who each performed the observer

study twice, with the two readings separated by at least 2 months to eliminate errors due to recollection of regions selected during the previous reading. Histograms of the intersection/union ratios for the reproducibility studies and for a comparison of two different radiologists are shown in Figures 1-3, below.

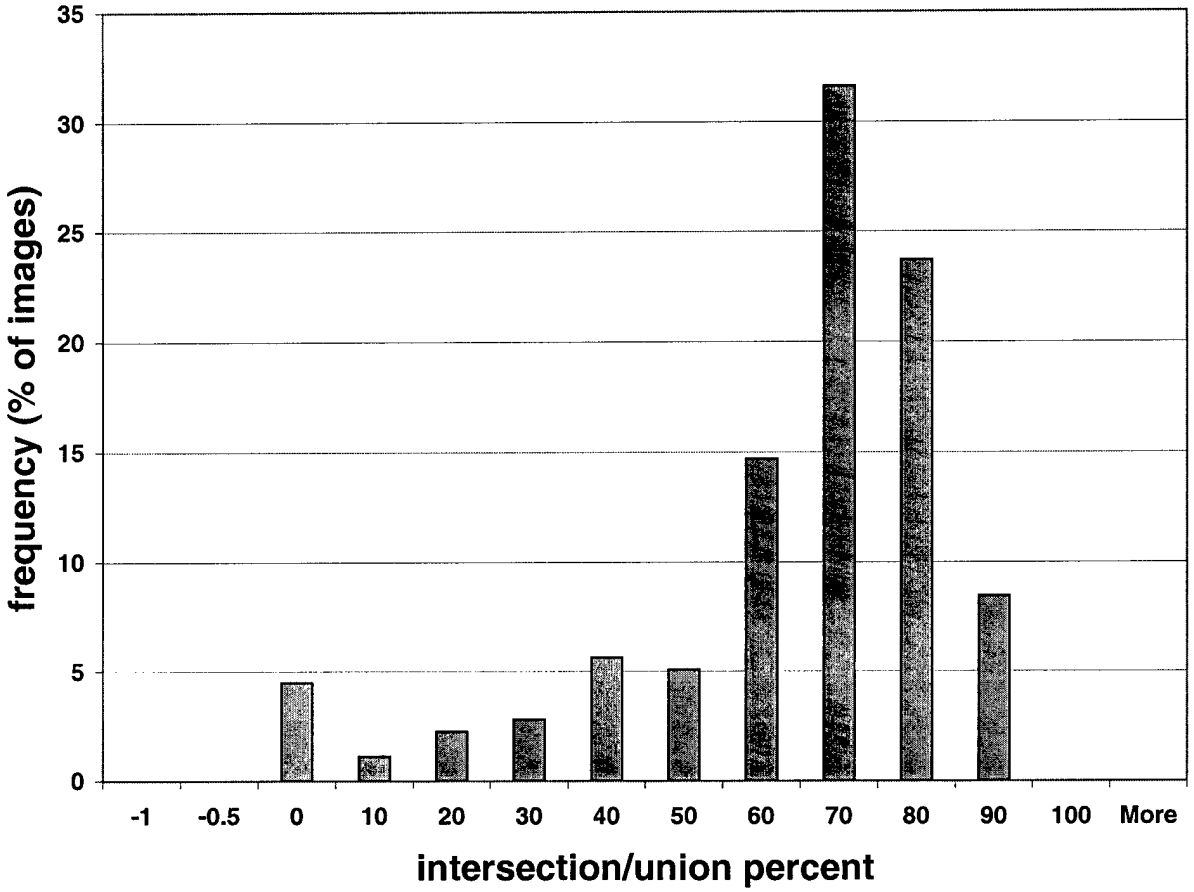

Figure 1. Histogram of largest intersection/union area percentages for regions in each image selected by one radiologist who performed the observer study twice. This plot represents the reproducibility of the regions selected by the radiologist. Notice that in about 32% of the images, the ratio of the largest ratio of the intersection of the regions selected divided by the union of the regions selected was about 70%, and in about 4% of the images, the intersection/union was 0. The mean value of the largest intersection/union ratios for this radiologist's analysis of all images is 59%.

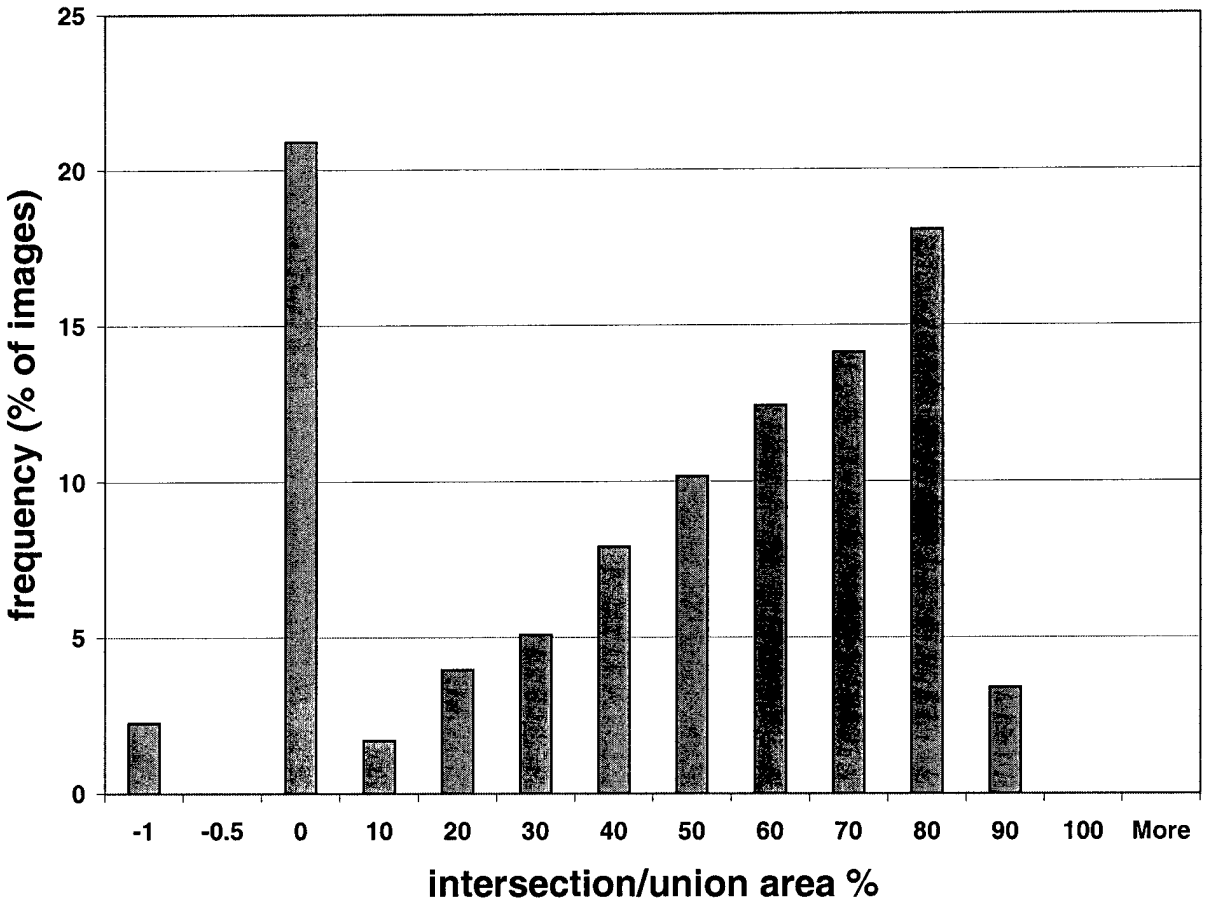

Figure 2. Histogram of largest intersection/union area percentages for regions in each image selected by a second radiologist who performed the observer study twice. This plot represents the reproducibility of the regions selected by this second radiologist. Notice that in about 18% of the images, the ratio of the largest ratio of the intersection of the regions selected divided by the union of the regions selected was about 80%, but in about 21% of the images, the intersection/union was 0. Also this radiologist did not select any regions during either study in about 2% of the images. This is represented by the intersection/union value of –1 in the above plot. The mean value of the largest intersection/union ratios for this radiologist's analysis of all images is 43%.

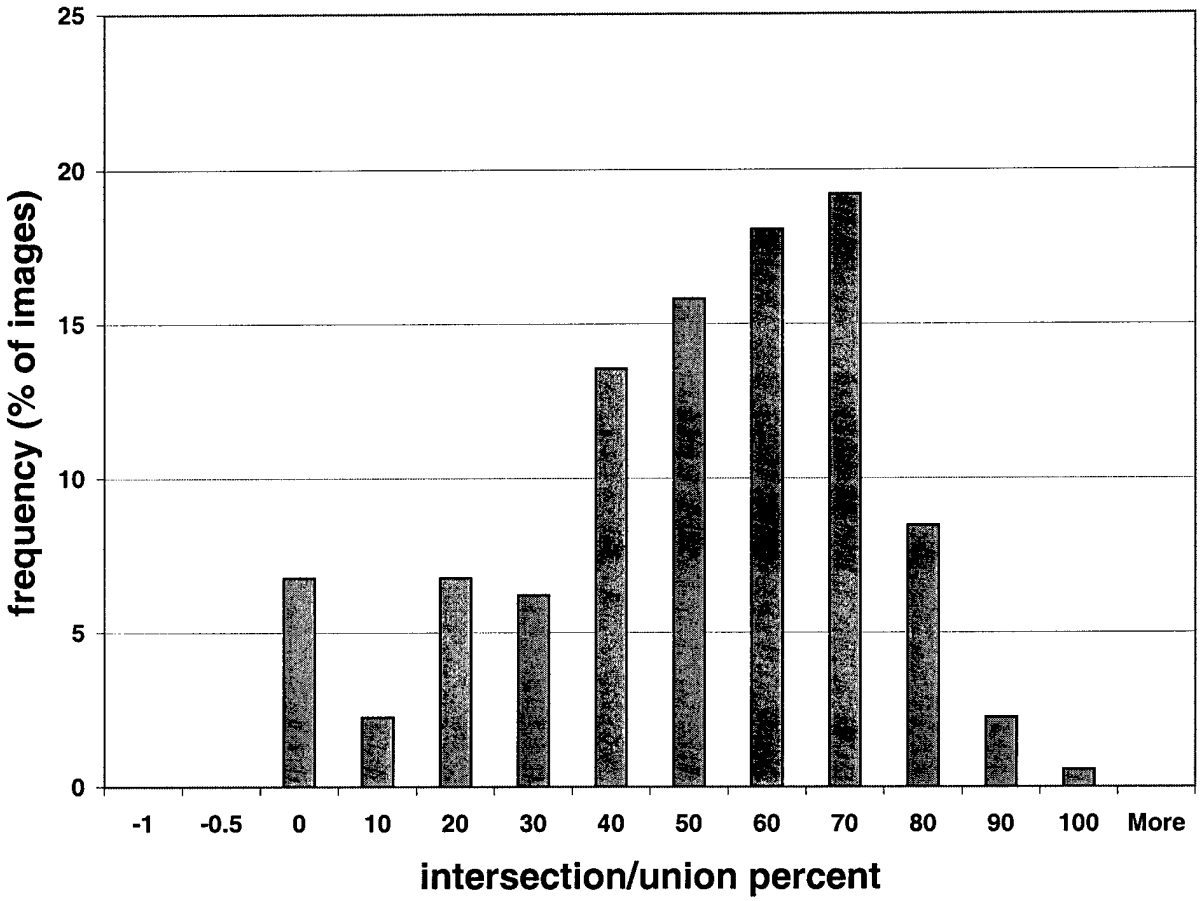

Figure 3. Example of histogram of largest intersection/union area percentages for regions in each image selected by two different radiologists. Notice that in about 18% of the images, the ratio of the largest ratio of the intersection of the regions selected divided by the union of the regions selected was about 70%, but in about 7% of the images, the intersection/union was 0. The mean value of the largest intersection/union ratios for this radiologist's analysis of all images is 46%.

A summary of the results is listed in Table 1, below.

Table 1: Intersection/Union Areas of regions for spot imaging selected by radiologists. Results for all combinations of 4 radiologists analyzed in pairs.

	Largest mean intersection/union	Second largest mean intersection/union
Average	37%	10%
Standard Deviation	8%	3%
Minimum	28%	6%
Maximum	46%*	16%
Reproducibility Radiologist #1	59% **	27%
Reproducibility Radiologist #2	43%***	18%

* Corresponds with histogram in Figure 3
** Corresponds with histogram in Figure 1
*** Corresponds with histogram in Figure 2

We conclude from Table 1 that there is fairly good agreement amongst the radiologists in their selection of suspicious dense regions for spot imaging. This agreement is not quite as good as the agreement between the regions selected by the same radiologist when he or she performed the study twice, but the values are comparable.

As reported last year, all of the radiologists commented that while the low resolution (800 micron pixel) images that were employed in the observer study were adequate for assessing suspicious dense regions, they would have preferred higher resolution images to assess architectural distortions, which are also spot imaged. During the third year of the project, we modified the software to display both 200-micron resolution and 400 micron resolution images. These images were obtained by down-sampling the original 50-micron resolution images. The 200-micron images were too large for our 1024 x 768 pixel display, so we developed software to permit the user to pan the image using scrollbars so that the entire image could be evaluated. Examples of the 200-micron and 400-micron resolution images of the same digitized mammogram are shown in Figure 4. This mammogram is one of a set of 200 new images that are being employed in a new observer study using higher resolution images. The red polygons that are shown in Figure 4 are those that were traced by one of the radiologists participating in the observer study. The green rectangles are the spot paddle regions corresponding to the red polygons. As in the previous program, the radiologist can adjust the sizes of the green rectangles with a pull down control in the program that increases the sizes in increments of 1-mm. This particular radiologist chose to employ green rectangles that just bordered the traced polygons (increment = 0 mm).

Figure 4: Example of 400-micron (left) and 200-micron (right) images that are being employed in a second observer study. Note that the 200-micron image can be panned using the slider controls at the bottom and right side of the image.

Finally, during the third year of this project, we applied computer aided diagnosis (CAD) algorithms developed by co-investigator Professor Heang-Ping Chan and her CAD group to the same set of digitized mammograms. For this application, we employed a threshold such that 3 or fewer dense regions were selected by the computer in each image. We are treating the computer as another reader in our observer study. Comparisons of the regions chosen by one of the radiologists and the computer in two of the images are shown in Figure 5, below.

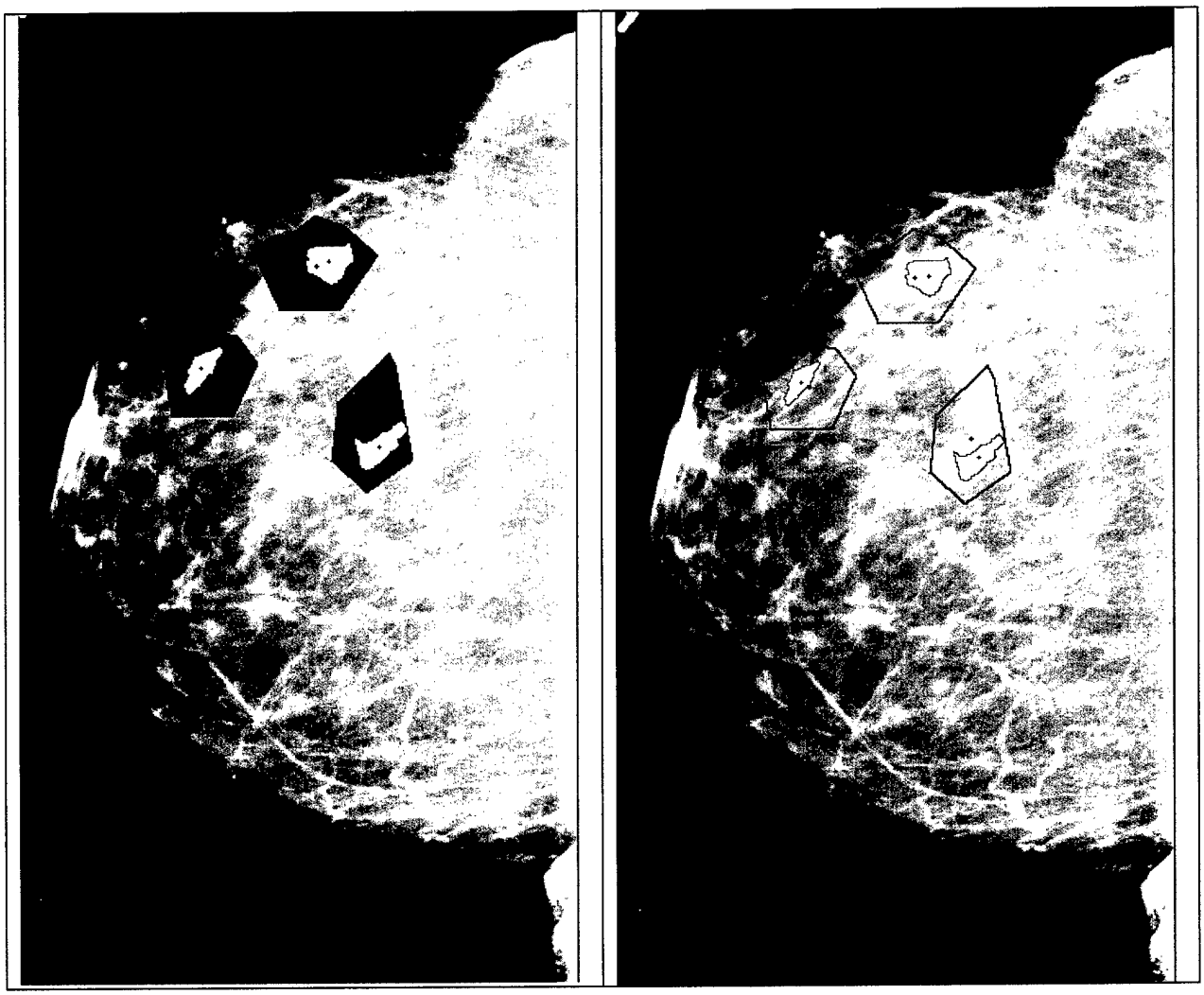

Figure 5. Regions selected by a radiologist and the CAD algorithm in the new observer study. In the image on the left, the regions selected by radiologist are painted red and those selected by the computer are painted green. The intersections are displayed in yellow. In this case the computer-selected regions are entirely encompassed by those selected by the radiologists, so all of the green regions appear as yellow. The outlines of the regions are shown in the image to the right.

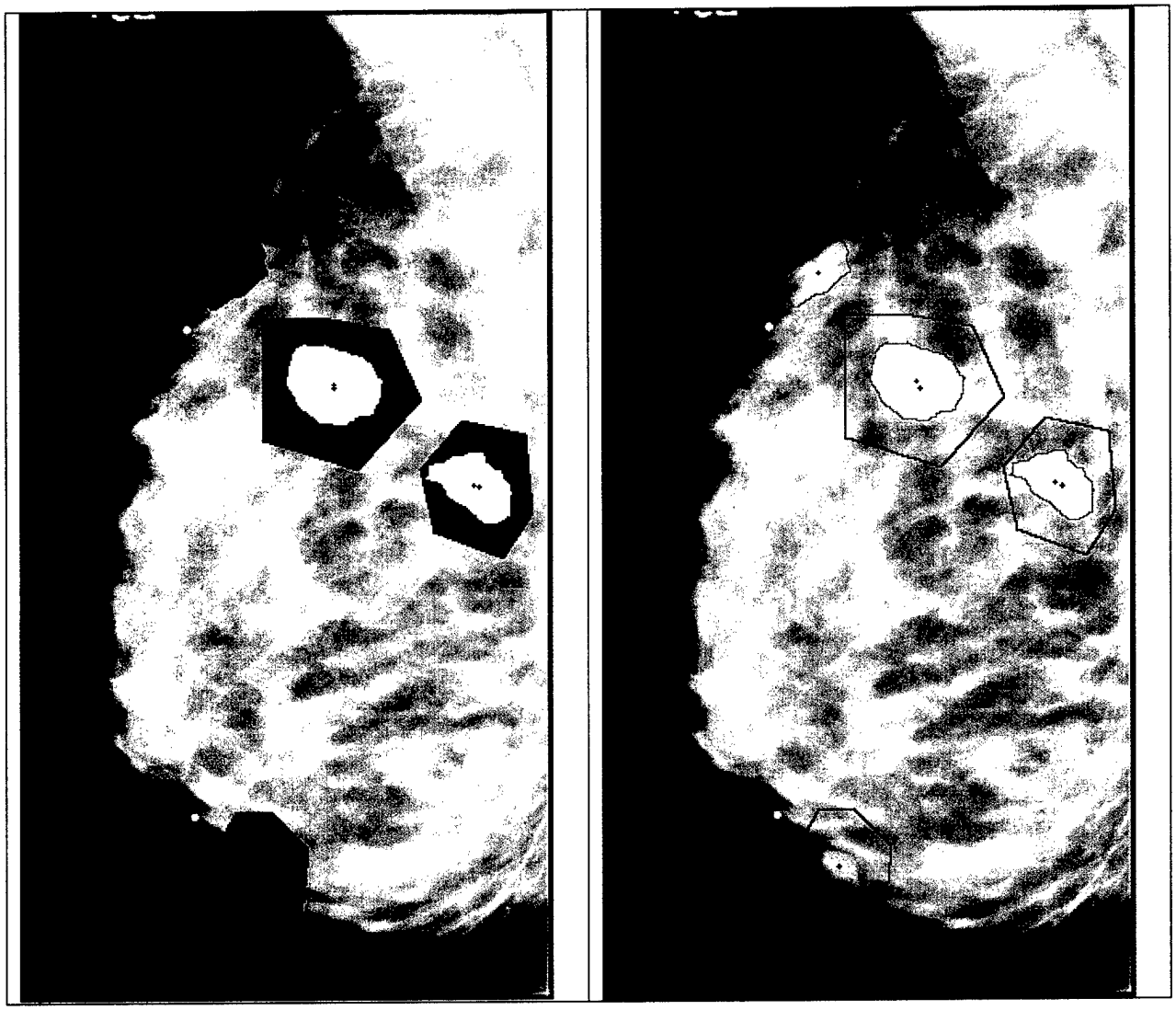

Figure 6. Regions selected by the radiologist (red) and computer (green) for another image in the observer study. In this case, the radiologist and computer agreed on two of the regions (intersection is in yellow in the image on the left), but differed on the third. The outlines of the regions are shown in the image on the right.

B) Task 2: Develop Secondary Collimator

The manufacturing of the secondary "spot" collimator was finished during the third year of this project. A photograph of the complete collimator is shown in Figure 7, and the separated longitudinal and transverse blade sections are shown in Figure 8.

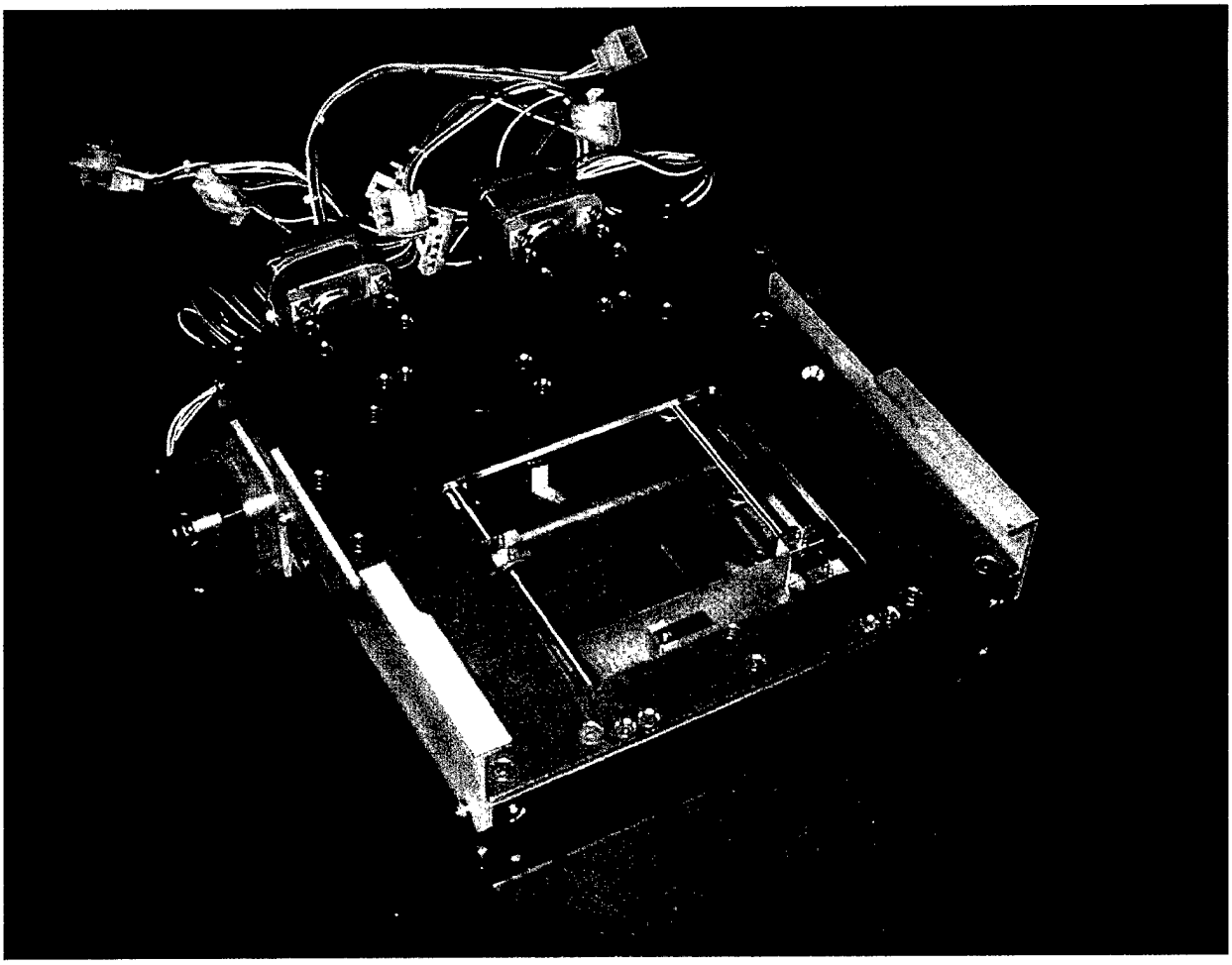

Figure 7: Photograph of the spot collimator that was developed for this project. The blades for this collimator are driven with 4 stepper motors, which are also shown in the picture.

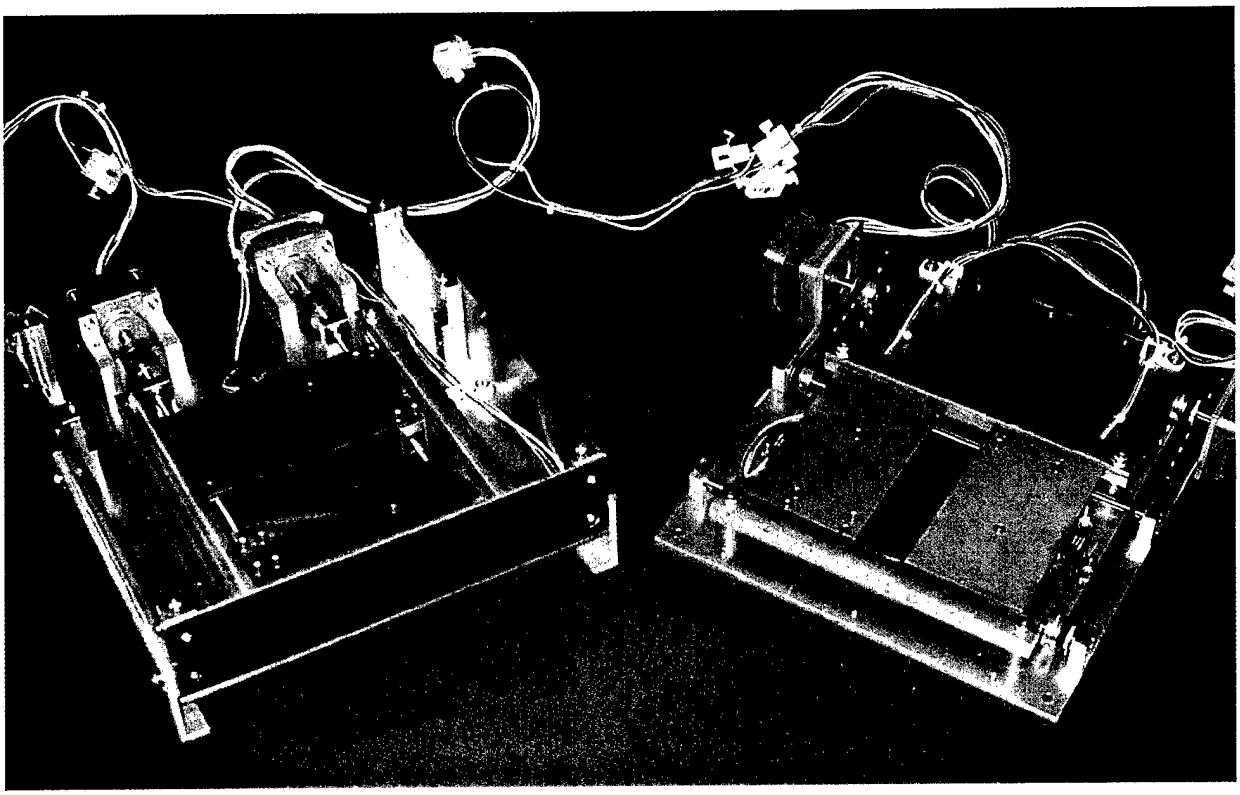

Figure 8: Photograph of the longitudinal and lateral collimator blades and their respective stepper motor drive mechanisms.

Software was written to "home" and position the collimator blades. The blade positions relative to the digital mammography image were calibrated by using several digital mammography images that were acquired with the blades at known numbers of steps beyond the "home" positions when the collimator was physically attached to the GE full-field digital mammography system

Another computer program was written which displays a full-field digital mammography image, and allows the user to position a rectangle in that image that represents the region for spot imaging. This program includes controls to adjust the contrast of the image and the shape, size, and position of the rectangle. Furthermore, the program is interfaced to the stepper motor drives of the spot collimator and moves the blades to form the desired rectangular beam for spot imaging. Experiments were performed to verify the proper operation of this software. We imaged a CIRS breast phantom in a CC projection We transferred this image to our PC computer, displayed it with our software, selected a region for spot imaging, had the software move the blades to the computed locations and took the spot image. The results of this experiment are shown in Figure 9. The program was found to accurately move the collimator blades for spot imaging. In performing this experiment, we took images of breast phantoms using different x-ray tube target and filter combinations. An interesting and at first unexpected result was that the accuracy of postioning appeared to depend on the x-ray tube target used (either Molybdenum or Rhodium.) When the same target ws employed for the calibration and spot imaging, the blade positions were accurate, but they were not when a different target was used for spot imaging. The reason is that the x-ray tube targets are vertically displaced along the central axis of the mammograph unit. Therefore, for accurate blade positioning, it is necessary to have separate spot collimator blade calibrations for each x-ray tube target.

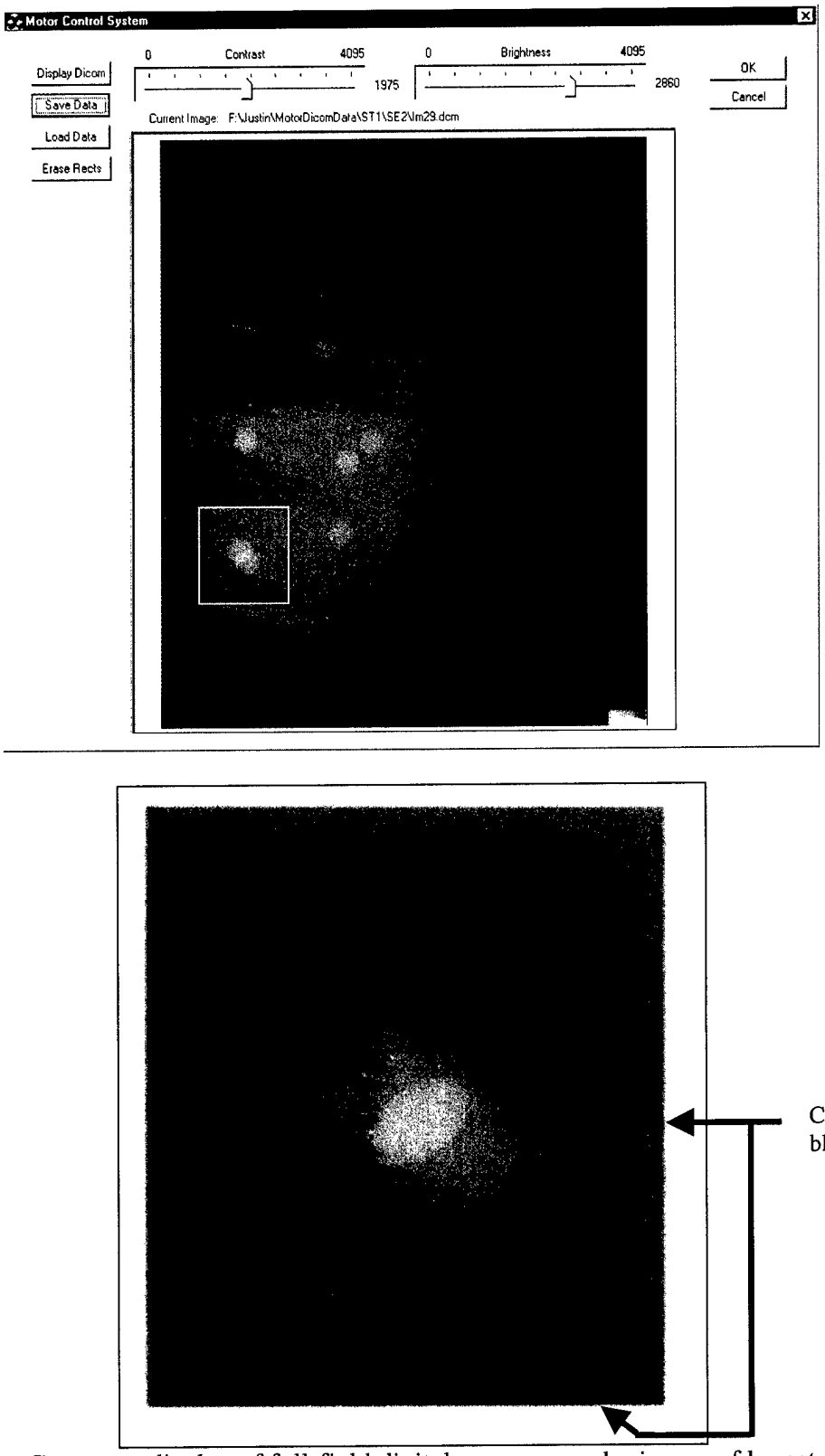

Figure 9: Top, Computer display of full-field digital mammography image of breast phantom with superimposed user selected rectangular region for spot imaging. Bottom: Zoomed representation of spot image acquired with spot collimator indicating proper operation of the spot collimation device.

It should be noted that the above experiment was not performed with the x-ray tube shifted to the left and right as will eventually be required for the full implementation of the stereo spot imaging technique. However, the experiment proved that spot collimator blades could be accurately positioned, relative to the image, which is necessary for that implementation. Calibration of the blades in the shifted x-ray tube positions will be performed during the extended year of this project.

C) Task 3: Develop system to restrain breast during changeover from full-field to spot compression paddle and reduce tension as spot paddle presses against breast.

A prototype system for accomplishing this task was designed and built during the first year of the project . Since we changed our approach as described in the Modified Statement of Work, such a device is not necessary for the new stereo spot technique that we are pursuing. Therefore, there was no further development of this device during the third year of the project.

D) Task 4: Develop system to position spot compression paddle

A prototype spot paddle positioner was designed and built during the first year of the project. This device is also not needed for the new stereo spot technique that we are pursuing. Therefore, there was no further development of this device during the third year of the project.

E) Task 5: Evaluate Automated Exposure Optimization (AOP) techniques for spot imaging application on commercial full-field digital mammography device.

Because the machinist did not finish manufacturing the spot collimator until September 6, 2002 and our project end date was September 14, 2002, we were not able to begin our evaluation of the AOP techniques with stereo spot imaging that was planned for the third year. This is one of the reasons we applied for a one-year no cost extension of this project. This extension was approved, and we plan to perform the AOP stereo spot studies during the fourth year of our project.

F) Task 6: Develop breast phantoms

Due to the late date that the machinist finished manufacturing the spot collimator mentioned in part (E) above, and our previous experience with the fairly rapid deterioration of the compressible breast phantoms, we did not pursue designing or having new compressible phantoms built for our studies. We have discussed the deterioration of the phantoms with the manufacturer, CIRS, Inc., and they are investigating different materials for the manufacture of more stable phantoms. We will design the phantoms and have them constructed during the approved fourth year of this project.

G) Task 7: Explore possible advantages of using stereo-spot mammography instead of single-projection, spot compression with spot collimation mammography for imaging overlapping structures

This task was completed during the second year of the project, and reported on in the second year annual report. We performed further analysis of the results and presented them during the third year of the project at the American Association of Physicists in Medicine (AAPM) meeting in Montreal, Canada, July 14-18, 2002,[1] and at the ERA of Hope meeting in Orlando, Florida, September 25-28, 2002. [2,3]

H) Task 8: Compare Contact and magnification stereomammography

We finished this task during the third year of the project. We wrote a paper on our investigation of depth measurements made with 3-D stereo cursors. . That paper, entitled "The effects of stereo shift angle, geometric magnification and display zoom on depth measurements in digital stereomammography, " has been accepted by Medical Physics and is currently in press. It will be published in the November, 2002 issue. [4] A proof copy of the paper is included in the appendix of this report. We also presented the results of our study comparing the ability of observers to distinguish positions of simulated fibrils at different radiation doses, stereo angles, and geometric magnifications in a poster at the SPIE-Medical Imaging meeting at San Diego, CA in February, 2002) [5]and at the ERA of Hope Meeting [6].

I) Task 9: Develop and implement changes in automated spot collimator design for prototype spot stereo mammography image acquisition system.

Although we obtained the completed spot collimator from the machinist very late during the third year of our project, we were able to calibrate it for single projection cranial caudal (CC) imaging. Some of our results are displayed in figure 9 of this report. Very recently, we have also acquired stereo projection images with the spot collimator and will calibrate the collimator blade positions for the stereo application using a technique similar to that used for the single CC projection. From the results of the single projection calibration, we learned that separate calibrations will have to be performed for each of the molybdenum and Rhodium x-ray tube targets, and this will be performed for stereo acquisition as well.

J) Task 10: Design second generation auto stereo spot mammography system

This final task will be performed during the fourth year of the project after we have gained more experimental experience with our first generation auto stereo spot mammography system.

(6) Key Research Accomplishments

- Further developed a computer program that enables radiologists to trace borders of suspicious regions worthy of spot imaging in digitized mammograms. The primary changes were to permit display of the images at higher resolutions – both 400-micron and 200-micron pixels. For the display of 200-micron resolution images, we developed algorithms to permit panning of the image so all portions of the digitized mammogram could be analyzed.

- Wrote software to compare the regions selected by the radiologists. This software computed all possible intersections of the regions selected and corresponding unions of the regions selected, and determined the intersection/union ratios ordered from largest to smallest for each image and for each combination of radiologists taken two at a time. The program automatically sends the results to an Excel spreadsheet for statistical analysis.

- Completed analysis of results for first observer study, which involved lower resolution (800 micron) images.

- Began second observer study using higher resolution images and also using regions selected by the computer using in-house developed computer aided diagnosis (CAD) techniques

- Completed development of automated spot collimator. Wrote computer program to move collimator blades via a stepper motor controller. Calibrated the collimator blade positioner from images obtained with the spot collimator attached to the full field digital mammography unit. Wrote computer program to permit user to select a rectangular region in a full field digital mammogram for spot imaging Tested this program with spot collimator using single projection images. Acquired stereo spot images for future calibration of collimator blade positions in the stereo spot application.

- Investigated effects of stereo shift angle, geometric magnification and display zoom on depth measurements made in stereo mammograms using in-house developed 3D cursors. Found best results were obtained with stereo shift angle of +/- 6^{o} and geometric magnification of 1.8, and that display zoom was not beneficial

- Compared observers' abilities to distinguish relative depths of simulated fibrils at different radiation doses, stereo angles, and geometric magnifications. Found significant improvements for stereo shift angle of +/- 6 vs +/-3 degrees, and geometric mag of 1.8x vs. Contact (mag ~ 1). Also, for large stereo shift angle and geometric mag, results were less dependent upon x-ray dose

- Based upon the above two stereomammography investigations, we conclude that the best stereo technique for the spot implementation would entail use of a stereo shift angle of +/- 6 degrees, geometric magnification of about 1.8, and half the dose of a conventional mammogram for each image of the stereo pair (total dose = dose of conventional mammogram).

(7) Reportable Outcomes

Manuscripts

MM Goodsitt, HP Chan, KL Darner and LM. Hadjiiski. The Effects of Stereo Shift Angle, Geometric Magnification, and Display Zoom on Depth Measurements in Digital Stereomammography In Press, to be published in the November issue of Medical Physics 2002

Abstracts and Presentations

Goodsitt M, Chan H-P, Gandra C, Chen N, Helvie M, Klein K, Bailey J, Paramagul C. Automated Spot Mammography: A Comparison of Spot Imaging Regions Selected by Radiologists. Presented at the 44th Annual Meeting of the American Association of Physicists in Medicine in Montreal, Quebec, Canada, July 14-18, 2002.(Medical Physics 2002;29:1307)

Chan HP, Goodsitt M, Hadjiiski L, Helvie M, Bailey J, Klein K, Roubidoux M. Development of digital stereo imaging technique for mammography. Poster presentation at the Era of Hope, Department of Defense Breast Cancer Research Program Meeting in Orlando, Florida, Sept 25-28, 2002. P28-6 in Proceedings, Volume II.

Goodsitt MM, Chan HP, Gandra CR, Chen NG, Helive MA. Automated stereo spot mammography for improved imaging of dense breasts. Poster presentation at the Era of Hope, Department of Defense Breast Cancer Research Program Meeting in Orlando, Florida, Sept 25-28, 2002. P28-11 in Proceedings, Volume II.

Goodsitt MM. Automated Stereo Spot Mammography for Improved Imaging of Dense Breasts. Presented in a Symposium entitled Digital Imaging: Diagnostic Potential and Enhancing Availability at the Era of Hope, Department of Defense Breast Cancer Research Program Meeting in Orlando, Florida, September 25-28, 2002. Page 30 of Program.

Chan HP, Goodsitt MM, Hadjiiski L, Bailey JE, Klein K, Darner KL, Paramagul C. Digital stereomammography: observer performance study of the effects of magnification and zooming on depth perception. Proc SPIE 4682. 2002: 163-166.

CONCLUSIONS

During the third year of this project, we have pursued developing the automated stereo spot imaging technique for improved visualization of dense regions in mammograms. This is the technique that we concluded during our second year would be more practical and offer superior visualization of superimposed structures than our originally planned method of combining spot automated spot compression with automated spot collimation. We continued our studies comparing the suspicious regions that different radiologists would choose for spot imaging. Based on feedback from radiologists who participated in our observer study of these regions that we performed during the second year of the project, we modified our computer programs to

display higher resolution images. This was needed for better perception of architectural distortions. We are using this modified display program in a new observer study, which in addition includes a comparison of the regions selected by the computer using in-house developed CAD techniques with the regions selected by the radiologists. The machinist finished manufacturing our spot collimator near the end of the third year of the project. The collimator is very well made and attaches easily to the GE Senographe 2000D full field digital mammography unit. We have written computer programs to move the blades of the spot collimator, to allow a user to interactively select a rectangular region within a full-field digital mammogram for spot imaging, and to have the collimator blades automatically moved to the correct locations to restrict the x-ray beam to expose only the desired spot region. We have tested the operation of the automated spot technique via images of a phantom containing simulated masses and found the spot collimator to be very accurate. During the third year, we also performed two major studies evaluating stereo mammography. In one, we determined the effects of stereo shift angle, geometric magnification and display zoom on the accuracies of depth measurements made in stereomammograms. We found the most accurate results were obtained with a +/- 6^{o} stereo shift angle and with geometric magnification of 1.8X. In another study, we compared the abilities of observers to distinguish relative depths of overlapping simulated fibrils (e.g. fibril A is in front of fibril B) " at different radiation doses, stereo angles, and geometric magnification factors. Based on the results of both studies, we conclude that depth perception in stereo spot mammography would be best using a +/- 6 degree stereo shift angle, geometric magnification of about 1.8X, and about half the dose of a conventional mammogram for each image of a stereo pair (total dose = dose of a conventional mammogram). It should be noted that since only part of the breast is imaged, in the spot technique, the effective dose would be less than that of a conventional mammogram by about the ratio of the volume of the tissue exposed with the spot technique to the volume of the tissue exposed with the full-field mammography technique. Because the finished spot collimator was obtained so late during the third year of the project (only 8 days before the end of the third year), we were not able to complete some of the planned tasks. (e.g., tasks 5, 6, 9 and 10) We requested a no cost one-year extension on our grant and this was approved. We will complete our unfinished work during the fourth year of this project.

So What

A key limitation of conventional x-ray mammography is the inability to optimally image regions of dense and overlapping tissue. The new full-field digital mammography systems reduce but not entirely eliminate this problem. Additional views including spot imaging are still employed with the digital systems to better analyze suspicious tissue regions. The system we are developing adds 3 features that will further optimize spot imaging of suspicious tissue. First a computer vision techniques will be employed to automatically find suspicious regions that warrant spot imaging. Second, the system will automatically collimate the x-ray beam to the suspicious region. This will reduce the amount of x-ray scatter that strikes the detector thereby reducing image noise. It should also restrict the region in which the automated technique and phototiming is determined, which may improve the penetration of this region. Third, the spot image will be acquired using a stereoscopic method. This will produce a 3-D image allowing the radiologist to see the depth separation between lesions and overlapping tissues and allowing the radiologist to see through any "cloud" of dense tissue. Stereoscopic imaging also permits improved visualization of the locations of lesions and microcalcifications and of lesion borders, all of which are important to the radiologists in making their diagnoses. Finally, the automated spot collimation stereo mammography technique is performed with the breast in the same location as in the full-field mammogram, eliminating the guesswork associated with breast re-positioning in conventional spot compression mammography. Thus, in theory, the automated

spot collimation, stereomammography technique should be of great benefit. The challenge will be to develop a convenient and practical system, which is the long-term goal of our project

(9) REFERENCES

1) Goodsitt M, Chan H-P, Gandra C, Chen N, Helvie M, Klein K, Bailey J, Paramagul C. Automated Spot Mammography: A Comparison of Spot Imaging Regions Selected by Radiologists. Presented at the 44th Annual Meeting of the American Association of Physicists in Medicine in Montreal, Quebec, Canada, July 14-18, 2002.(Medical Physics 2002;29:1307)

2) Goodsitt MM, Chan HP, Gandra CR, Chen NG, Helive MA. Automated stereo spot mammography for improved imaging of dense breasts. Poster presentation at the Era of Hope, Department of Defense Breast Cancer Research Program Meeting in Orlando, Florida, Sept 25-28, 2002. P28-11 in Proceedings, Volume II.

3) Goodsitt MM. Automated Stereo Spot Mammography for Improved Imaging of Dense Breasts. Presented in a Symposium entitled Digital Imaging: Diagnostic Potential and Enhancing Availability at the Era of Hope, Department of Defense Breast Cancer Research Program Meeting in Orlando, Florida, September 25-28, 2002. Page 30 of Program.

4) MM Goodsitt, HP Chan, KL Darner and LM. Hadjiiski. The Effects of Stereo Shift Angle, Geometric Magnification, and Display Zoom on Depth Measurements in Digital Stereomammography In Press, to be published in the November issue of Medical Physics 2002

5) Chan HP, Goodsitt MM, Hadjiiski L, Bailey JE, Klein K, Darner KL, Paramagul C. Digital stereomammography: observer performance study of the effects of magnification and zooming on depth perception. Proc SPIE 4682. 2002: 163-166.

6) Chan HP, Goodsitt M, Hadjiiski L, Helvie M, Bailey J, Klein K, Roubidoux M. Development of digital stereo imaging technique for mammography. Poster presentation at the Era of Hope, Department of Defense Breast Cancer Research Program Meeting in Orlando, Florida, Sept 25-28, 2002. P28-6 in Proceedings, Volume II.

(10) Appendix

The following publications in the current year as a result of this grant are enclosed with this report.

1) MM Goodsitt, HP Chan, KL Darner and LM. Hadjiiski. The Effects of Stereo Shift Angle, Geometric Magnification, and Display Zoom on Depth Measurements in Digital Stereomammography In Press, to be published in the November issue of Medical Physics 2002

2) Chan HP, Goodsitt MM, Hadjiiski LM, Bailey JE, Klein K, Darner KL, Paramagul C. Digital stereomammography: Observer performance study of the effects of magnification and zooming on depth perception. In: Medical Imaging 2002: Physics of Medical Imaging, Larry E. Antonuk and Martin J. Yaffe, editors, Proceedings of SPIE, vol. 4882, 2002, pages 163-166.

3) Goodsitt M, Chan H-P, Gandra C, Chen N, Helvie M, Klein K, Bailey J, Paramagul C. Automated Spot Mammography: A Comparison of Spot Imaging Regions Selected by Radiologists. Presented at the 44th Annual Meeting of the American Association of Physicists in Medicine in Montreal, Quebec, Canada, July 14-18, 2002. (Medical Physics 2002;29:1307)

4) Goodsitt MM, Chan HP, Gandra CR, Chen NG, Helvie MA. Automated stereo spot mammography for improved imaging of dense breasts. Poster presentation at the Era of Hope, Department of Defense Breast Cancer Research Program Meeting in Orlando, Florida, Sept 25-28, 2002. P28-11 in Proceedings, Volume II.

5) Chan HP, Goodsitt M, Hadjiiski L, Helvie M, Bailey J, Klein K, Roubidoux M. Development of digital stereo imaging technique for mammography. Poster presentation at the Era of Hope, Department of Defense Breast Cancer Research Program Meeting in Orlando, Florida, Sept 25-28, 2002. P28-6 in Proceedings, Volume II.

The effects of stereo shift angle, geometric magnification and display zoom on depth measurements in digital stereomammography

Mitchell M. Goodsitt,[a] Heang-Ping Chan, Katie L. Damer, and Lubomir M. Hadjiiski
Department of Radiology, University of Michigan, Ann Arbor, Michigan 48109-0030

(Received 23 January 2002; accepted for publication 15 August 2002; published 28 October 2002)

We are developing virtual three-dimensional (3-D) cursors for measuring depths in digital stereomammograms. We performed a study to investigate the effects of stereo shift angle, geometric magnification, and display zoom on the accuracy of depth measurements made with a virtual 3-D cursor. A phantom containing 50 low contrast fibrils at depths ranging from 1 to 11 mm was imaged with a full-field digital mammography system. Left- and right-eye images were generated at stereo shift angles of ±3° and ±6°, using either contact or 1.8× geometric magnification geometry. The images were viewed on a high-resolution stereoscopic display system in normal and 2× zoom mode. Observers viewed the images with stereo glasses and adjusted the depth of a cross-shaped virtual cursor to best match the perceived depth of each fibril. The results for two trained observers with excellent stereo acuity were nearly identical when viewing the same images. The average root mean square errors for the two observers were 1.2 mm (±3° contact, no zoom), 1.3 mm (±3° contact zoom), 0.8 mm (±6° contact, no zoom), 0.6 mm (±6° contact, zoom), 0.8 mm (±3 magnification, no zoom), 0.7 mm (±3° magnification, zoom), and 0.2 mm (±6° magnification, no zoom). One observer repeated the entire study for two additional fibril phantom configurations. Combining all the results, we found that for the contact geometry increasing the stereo shift angle from ±3° to ±6° improved the depth measurement accuracy by factors of about 1.2–4.0. Zooming did not provide observable improvement in the depth measurement accuracy; sometimes having no effect, sometimes improving the accuracy, and other times reducing the accuracy, with no general trends. Its effect is likely within experimental errors. However, the stereo effect was more readily visualized in the zoom mode. Geometric magnification improved the depth measurement accuracy. The best accuracy among all cases was about 0.2 mm, obtained with geometric magnification using a stereo angle of ±6°. This is the mode we recommend for obtaining accurate depth measurements with virtual cursors in stereomammograms. © *2002 American Association of Physicists in Medicine.* [DOI: 10.1118/1.1517615]

Key words: stereomammography, stereoscopic, virtual cursor, 3-D imaging

I. INTRODUCTION

Tissue superposition makes it difficult to accurately interpret conventional mammograms. Such mammograms are acquired using a single projection method whereby (ignoring scatter) the density at a point in the image represents the summation of the attenuation of all tissues along a ray extending from the x-ray tube focal spot to that point. The superpositon of tissues along the rays decreases image contrast and can result in the camouflaging of masses and microcalcifications within dense tissue. It can also lead to superimposed structures having mass-like appearances. The superpositon problem can be reduced or eliminated by generating and viewing 3-D mammograms via multiprojection techniques such as stereoradiography,[1–7] tomosynthesis,[8–10] and computed tomography.[11,12]

We have been investigating digital stereomammography. This is a computerized version of an analog technique that was first described by Warren in 1930.[13] Both the new and old techniques involve taking two separate mammograms, one with the x-ray tube at a positive angle (e.g., +3°) relative to a normal to the detector and the other with the x-ray tube at an equal but opposite angle (e.g., −3°) about the normal. One of the images is viewed with the left eye and the other with the right eye. Our brain fuses the images together to create a 3-D effect. The old technique required taking two films in roughly the same projection. As such, it had several disadvantages, including at least twice the x-ray dose, film cost, and processing time. It also required increased procedure time and radiologist viewing time. Radiologists, in general, eventually decided that these disadvantages outweighed the 3-D visualization advantage, and film stereomammography was discontinued. Digital mammography eliminates or reduces most of these advantages, thereby making digital stereomammography a potentially viable technique. In contrast to screen-film systems, which have sigmoid-shaped response curves, digital detectors have a linear response. Thus, the response curve of the digital detector does not degrade image contrast at lower doses, and it may be possible to utilize half the normal dose for each digital image. The two images of the stereo image pair will be integrated by the observer's eye–brain system to yield about the same signal-to-noise ratio as in a single image taken with the same total dose.[14] With digital systems, image processing and display are almost instantaneous. Also, the method of examining the

 0094-2405/2002/29(11)/2725/10/$19.00

images, displayed on a television monitor and viewed with liquid crystal display (LCD) glasses that are synchronized so the left eye sees one image and the right the other, is more convenient and less time consuming than the film counterpart.

We have been investigating the use of virtual 3-D cursors for measuring depths in digital stereomammograms.[3,5,6] Leduc *et al.*[1] have also performed research in this area. The 3-D cursors are generated with computer graphics and are overlaid on the digital mammograms. In our initial studies reported previously,[3] we determined the accuracies of observers' measurements of the depths of horizontally and vertically oriented nylon filaments that simulate fibrils in mammograms. We found that when observers used a cross-shaped cursor, they could determine depths of vertically oriented fibrils with accuracies [root mean square (rms) errors] of 0.4–1.3 mm, but their accuracies were degraded for horizontally oriented fibrils (rms errors of 1.9–4.2 mm). In a subsequent study,[5] we found that use of a comb-shaped cursor improved the accuracies (reduced the rms errors) of observers' depth measurements of the horizontally oriented fibrils by 0.1–1.4 mm. With this cursor, two of the observers were able to measure the absolute depths of the horizontal fibrils with much improved accuracies of 0.8–1.0 mm. The images for our previous studies were generated with a Fischer (Denver, CO) MammoVision Stereotaxic unit, using a stereo shift of ±2.5°. More recently, our Radiology department obtained a GE (Milwaukee, WI) Senographe 2000D full-field digital mammography system. In this report, we describe a study that was performed using images acquired with this system. We investigated the effects to stereo shift angle, geometric magnification, and display zoom on the accuracy of depth measurements made with a virtual 3-D cursor.

II. MATERIALS AND METHODS

A. Phantom

We employed the same multi-layered fibril phantom that was used in our previous studies.[3,5,6] This phantom consists of six 1 mm thick Lexan sheets each separated by 1 mm spacers. A 5×5 matrix of 8 mm long, 0.53 mm diameter nylon fibrils is placed on the plates with 25 fibrils oriented vertically (perpendicular) and 25 horizontally (parallel) relative to the stereo shift direction. The depths and orientations of the fibrils were randomized and organized such that one horizontal fibril crossed one vertical fibril at each of the 25 matrix positions. The order of the Lexan layers could be changed to create many independent phantom configurations. For our present experiments, we rotated the phantom 45°. This resulted in 25 of the fibrils being oriented at +45° and 25 at −45° relative to the stereo shift direction. Thus, all fibrils had both horizontal and vertical components.

B. Stereo image acquisition

As mentioned above, the images were generated with a GE Senographe 2000D digital mammography system. The pixel size for this system is 100 μ in contrast to the 50 μ pixel size of our previous images obtained with the Fischer MammoVision stereotaxic unit. The GE system employs a digital detector consisting of a CsI:Tl light converter and an *a*-Si active matrix flat panel unit with photodiodes and TFT pixel switches.[15] The detector measures 23 cm×19 cm. Stereo images are traditionally produced by shifting the x-ray tube to the right and left of an axis perpendicular to the detector. Usually, the total x-ray tube shift is 10% of the focus-to-detector distance, which corresponds, with a stereo shift angle of about ±3° [$=\tan^{-1}(0.1/2)$]. For phantom imaging, an alternative to shifting the x-ray tube is shifting the phantom. This is illustrated in Fig. 1. We employed this method for all of the contact images in this study. We built a phantom sliding device with positioning marks at the locations for the two shift angles that were studied (±3° and ±6°). Note for illustration purposes, to simplify the comparison of the methods, that the x-ray tube in Fig. 1 is shown rotating about a fulcrum at the center of the detector, with a stereo shift angle, θ. In the calculation of the shift distance, w, for our phantom-shift imaging setup, the actual geometry was used (i.e., a source-to-detector distance of 66 cm, a fulcrum 46 cm from the focal spot, and a magnification-stand-to-detector distance of 26.4 cm). The small difference in the focus-to-detector and focus-to-object distances for the tube-shift and phantom-shift methods, when the tube shift involves x-ray tube rotation about a fulcrum, was neglected in our study. For the actual contact and magnification geometries that were employed, it can be shown that these differ-

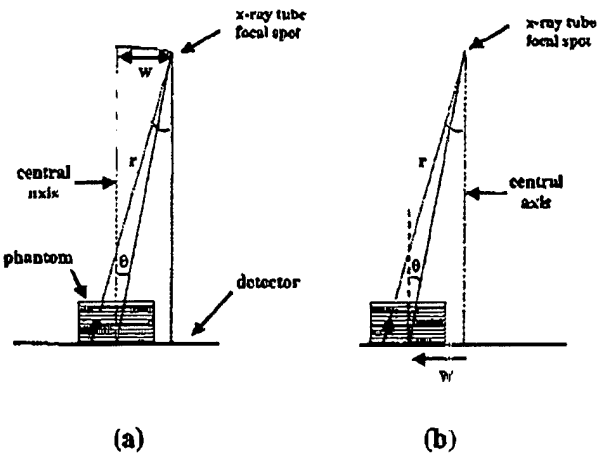

FIG. 1. Tube shift (a) and phantom shift (b) methods of stereo image acquisition. Both sketches illustrate the geometries for the generation of the right-eye images. In (a) the x-ray tube focal spot shifts a distance w to the right. In (b), the x-ray tube focal spot remains fixed along the central axis of the detector, and the phantom shifts a distance w to the left. The sketches illustrate the equivalency of the geometries of the two methods. Notice that they ray r passes through the black circular object in the phantom at the same angle in both cases. The corresponding drawing for the left-eye images of the stereo pairs would have the x-ray tube in (a) shifted to the left a distance w, and the phantom in (b) shifted a distance w to the right.

ences have a 0.6% or smaller effect on the accuracy of the results, which is essentially negligible (e.g., 0.6% of 1.0 mm accuracy=0.006 mm).

When using the tube-shift and phantom-shift methods, it is desirable to align the resulting images such that an object (e.g., a fibril) in contact with the bottom of the phantom does not shift. By doing so, all depths or distances of objects in the phantom will be measured relative to the back surface of the phantom. We achieved the desired zero shift by placing a fiducial marker on the top surface of the slider on which the phantom was placed and digitally translating the resulting left- and right-eye images so that the fiducial markers coincided. For magnification mammography, especially at larger stereo shift angles, the phantom shift method cannot be used because only a portion of the phantom will project to within the field of view of the detector due to the limited size of the detector. For our magnification techniques, we employed the phantom-shift method for the ±3° stereo image acquisition and the tube-shift method for the ±6° stereo image acquisition. All images in this study were obtained using a technique of 30 kVp, Rh filter, Rh target, 63 mAs. The large (nominal 0.3 mm) focal spot was employed for the contact images and the small (nominal 0.15 mm) focal spot for the (1.8×) geometric magnification images. The scatter-rejection grid was removed for magnification image acquisition.

C. Stereo image display

The stereoscopic display system that was employed for this study consisted of a Barco-Metheus (Beaverton, OR) model 1760S stereo graphics board in a SUN Microsystems (Palo Alto, CA) Ultra 10 computer. The Metheus board operates in a page flipping stereoscopic mode whereby the left- and right-eye images are displayed sequentially, one after the other. This board is capable of displaying 1408×1408×8 bit progressive-scan images at a refresh rate of 114 Hz. The images in our study were displayed on a 21 in. Barco model 521 monitor and viewed with NuVision (Beaverton, OR) LCD stereoscopic glasses. We employed in-house developed software to display, pan, zoom, and adjust the contrast and brightness of the images.

D. Virtual cursor

We developed software to generate the virtual cursors and display their x, y, and z positions. The 3-D nature of the cursor is achieved by introducing offsets in the horizontal positions of the representations of the cursor in the left- and right-eye images. The z coordinate is equal to the offset. When the offset is 0, the cursor is at the same x, y position in both images, and it appears stereoscopically to be at the depth of the monitor screen. As the horizontal offset between the cursor positions is increased in one direction (e.g., left), the cursor appears to move closer to the observer, and as the offset is increased in the opposite direction (e.g., right), the cursor appears to move toward or into the monitor.

E. *Z*-coordinate calibration

The z coordinate was calibrated by imaging thin wires placed on the steps of a solid acrylic step wedge accurately milled with known step heights. The step wedge was imaged with the GE digital mammography system using the same phantom shift or x-ray tube shift as for the images of the fibril phantoms under the corresponding imaging conditions, and using the fiducial marker alignment technique described previously. The thin wires that were employed for calibration were oriented perpendicular to the tube shift direction. The resulting stereoscopic images were viewed without the stereo glasses and the left- and right-eye cursor positions were adjusted to overlay the left- and right-eye images of the wires on the steps. The z coordinates of the cursor were linearly fit to the known depths of the wires to obtain the calibration line. This calibration was performed for each of the image magnification/zoom conditions discussed below. While this calibration method is accurate and highly reproducible, it relies on the ability of the user to match the positions of the cursors and fibrils in the image and is therefore subjective. A future improvement of the calibration method would entail developing a computer program to determine the positions of the fibrils (e.g., their centers of masses).

F. True fibril depths

Through a careful examination of the fibril phantom, we noticed that minor warping of the sandwiched Lexan plates could cause the actual depths of the fibrils to differ from their nominal 1, 3, 5, 7, 9, and 11 mm values. To more accurately determine the true depths of the fibrils for each phantom layer configuration, we applied the calibration method described above to one set of the stereo pair images. The ±6° magnification image pair was selected because the displacements in the fibril locations between the left- and right-eye images are the greatest for this image pair. The larger displacement results in greater localization accuracy since the limitation of approximately ±1 pixel uncertainty in placement of the stereo cursors on the fibrils in the images will correspond to a smaller uncertainty in the actual depth. A third observer who was different from the two who participated in the observer study described below viewed, without the stereo glasses, the ±6° magnification stereo pair images of the phantoms in the three multilayer configurations studied and adjusted the left- and right-eye cursor components to overlay each fibril. The measured z values were then converted to true depths in millimeters using the calibration lines derived with the step wedge phantom. In performing this procedure, we found that when the nominal 1 mm depth fibrils (i.e., those that were a distance of 1 mm from the bottom of the phantom) were viewed without the glasses, they were too close to each other for the accurate positioning of overlaying cursors. We therefore could not determine their true depths and only analyzed the true depths of the fibrils at the nominal 3, 5, 7, 9, and 11 mm depths in the phantoms. Hence, the results in this paper are only presented at those depths. This is a consequence of the method that was employed to determine the true depths and would not be a limi-

tation for a test object that was perfectly flat at each level since the true depths would then be equal to the nominal depths.

G. Observer study

For the observer experiment, we arranged the multilayered phantom in one configuration, and had two participants use the stereoscopic virtual cursor system to measure the depths of the fibrils in stereomammograms of the phantom for the seven stereo angle/geometry/display conditions described in the following: (1) ±3° stereo, contact geometry, no zoom; (2) ±3° stereo, contact geometry, zoom =2×; (3) ±6° stereo, contact geometry, no zoom; (4) ±6 stereo, contact geometry, zoom =2×; (5) ±3° stereo, geometric magnification =1.8×, no zoom; (6) ±3° stereo, geometric magnification =1.8×, zoom =2×; and (7) ±6° stereo, geometric magnification =1.8×, no zoom.

In addition, one of the observers repeated the entire study for two other phantom configurations. That observer also made a second set of measurements on one of the images (contact geometry with ±6° stereo shift angle) 8 months after the initial reading to assess reproducibility.

The stereo acuity of both observers was tested using a standard Randot® Circles Stereo test (Stereo Optical Co., Inc., Chicago, IL). In this test, the subject views a set of ten objects on the test pattern through polarized glasses. Each object consists of three circles, one of which when viewed stereoscopically should appear to be closer to the observer than the other two. The test subject is asked to identify the circle that appears closest in each object. Both observers in our study accurately identified each circle that was closer to them for all cases, indicating their level of stereopsis is at least 20 s of arc at a viewing distance of 16 in. Their performance is comparable to the average (21.3 s of arc) that has been measured with this test pattern for adults with excellent, balanced monocular visual acuity (at least 20/20 in each eye and equal acuity in both eyes).[16]

The cursor that was employed in our studies was a black cross-shaped cursor. It was symmetrically shaped with an overall height of 64 pixels, and an overall width of 64 pixels. The lines were two pixels thick, and the arrowheads at each end of the lines were three pixels long. In a brief preliminary study, it was found that a cursor like this that has vertical and horizontal lines worked best for measuring the depths of the +45° and −45° oriented fibrils.

The observers recorded their measured z coordinates of each fibril, and these z coordinates were converted into depths (or actually distances in front of the back surface of the phantom) using calibration lines that were calculated from the step wedge data discussed above. These depths were then compared with the known depths both by performing linear least-squares fits and by computing the rms and mean errors. Parameters of linear least-squares fits that were compared for each observer for the seven stereo angle/geometry/display zoom combinations included the slope, intercept, correlation coefficient (r value), and standard error of the estimate (SEE). The rms errors were computed using the equation

$$\text{rms error} = \sqrt{\frac{\sum_{i=1}^{N}(\text{true depth}_i - \text{measured depth}_i)^2}{N}},$$

when N was the total number of fibrils excluding those at the nominal 1 mm depth (N was equal to 40 for one of the phantom configurations and 42 for the other two phantom configurations). Finally, two-tailed paired t tests of the differences between the measured and true z coordinates of the fibrils for the various stereo imaging/viewing techniques were performed to determine the statistical significance of those differences.

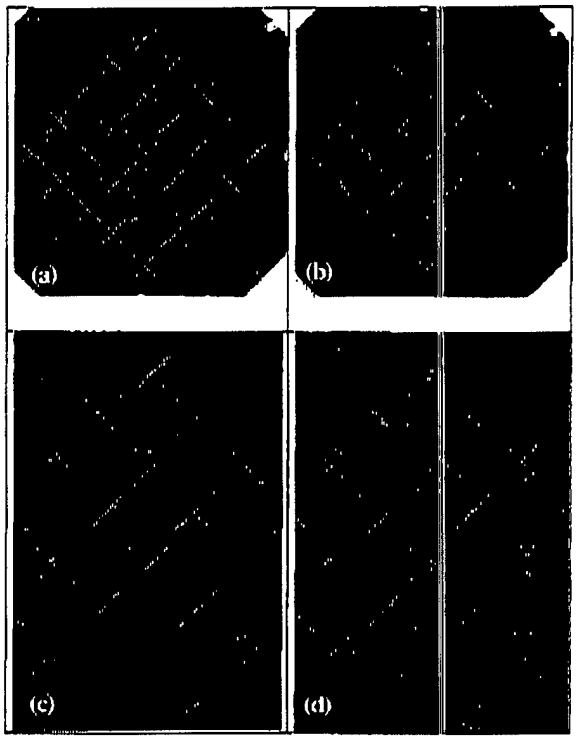

FIG. 2. Examples of images for (a) ±3° stereo shift angle, contact geometry, (b) ±6° stereo shift angle, contact geometry, (c) ±3° stereo shift angle magnification geometry, and (d) ±6° stereo shift angle magnification geometry. Note the combined images in this figure were created for illustration purposes by averaging the left- and right-eye images. In the actual stereo display, the left- and right-eye images are perceived individually. The averaging process helps illustrate the two images at once, but reduces the true image contrast.

III. RESULTS

Combined left-eye and right-eye images of the same phantom obtained with the following geometries: ±3° stereo shift—contact, ±6° stereo shift—contact, ±3° stereo shift—magnification, and ±6° stereo shift—magnification are shown in Fig. 2. Examples of the calibration lines that were computed from the step wedge measurements are shown in Fig. 3. The calibration lines for the ±3° and ±6° stereo shift angles in contact geometry are compared in part (a) of this figure, and the corresponding lines for the magnification ge-

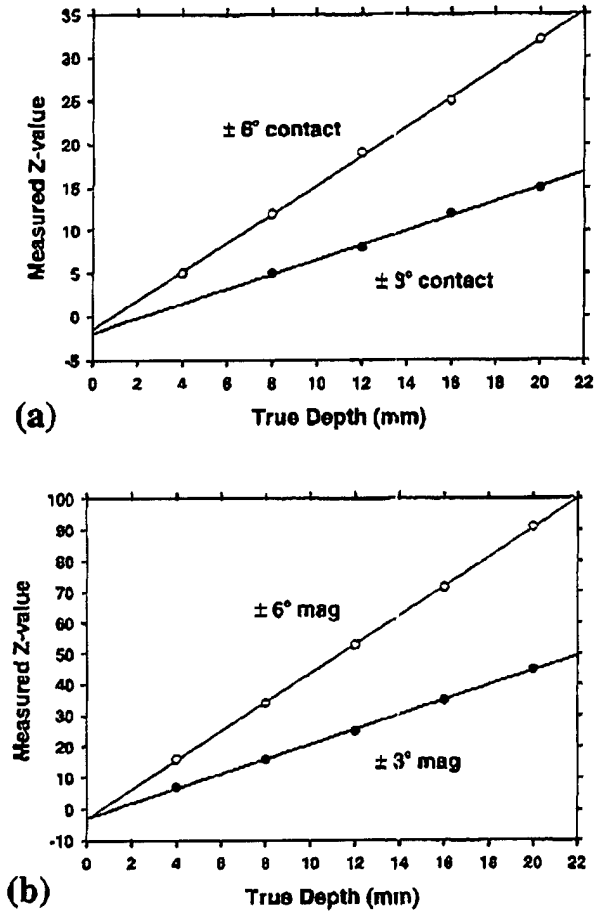

FIG. 3. (a) Calibration lines for ±3° stereo shift contact and ±6° stereo shift contact acquisition; (b) calibration lines for ±3° stereo shift magnification and ±6° stereo shift magnification acquisition.

ometry are compared in part (b). For the 2×-zoom mode, our cursor software effectively incremented the z values in steps of 0.5 per pixel shift instead of steps of 1 for the nonzoom mode. Consequently, the calibration lines that were computed in the 2×-zoom display modes were nearly identical to those in the nonzoom modes and they are therefore not shown in the figures. The calibration equations for the conversion of the measured z values to the depths (distances from the back of the phantoms) for the various imaging conditions are listed in Table I, below.

TABLE I. Calibration equations for converting measured z values to depths (distances in front of the backside of the phantom). *Note:* these calibration equations were derived by linearly fitting the data acquired from the step wedge images. Examples of the lines for the step wedge data are shown in Fig. 1.

Stereo Shift Angle	Geometry	Display zoom	Equation
±3 degrees	Contact	None	$\text{Depth (mm)} = \frac{Z+1.9}{0.85}$
±3 degrees	Contact	2×	$\text{Depth (mm)} = \frac{Z+1.55}{0.825}$
±6 degrees	Contact	None	$\text{Depth (mm)} = \frac{Z+1.5}{1.675}$
±6 degrees	Contact	2×	$\text{Depth (mm)} = \frac{Z+2.5}{1.75}$
±3 degrees	Magnification	None	$\text{Depth (mm)} = \frac{Z+2.9}{2.375}$
±3 degrees	Magnification	2×	$\text{Depth (mm)} = \frac{Z+2.6}{2.35}$
±6 degrees	Magnification	None	$\text{Depth (mm)} = \frac{Z+3.15}{4.688}$

Results comparing the performances of the two observers for the various stereo angle, geometric magnification, and display zoom combinations of the experiment are summarized in Tables II–IV. Examples of plots of the measured versus true depths for one observer for each of the imaging conditions are shown in Fig. 4. Errors in the depth measurements for each imaging condition for the one observer who viewed images in two additional phantom configurations are listed in Table IV. The paired t-test results for the observer who measured the z values of the fibrils in the phantom in three separate phantom layer configurations are listed in Table V. (Note, the paired t-test results for the other observer who made measurements of the fibrils in the first phantom configuration were very similar to those listed in part A of this table and are therefore not shown.)

The reproducibility of the observer's measurements in the same image read twice was excellent. For the 40 fibrils that were analyzed in the image, 35 of the measured z values were the same for both readings, and the remaining 5 z values differed by ±1. This translates to a rms difference in the z values of 0.354 (i.e., $\sqrt{5/40}$), which is equal to 0.21 mm.

TABLE II. Linear fit parameters for measured versus true depths of fibrils for two observers (values for observer 1 are indicated by subscript 1, and for observer 2 by subscript 2).

	3°	3° zoom	6°	6° zoom	3° mag	3° mag zoom	6° mag
r_1	0.956	0.949	0.994	0.996	0.982	0.978	0.998
r_2	0.934	0.921	0.994	0.996	0.985	0.981	0.998
intercept_1	0.669	0.030	−0.757	−0.306	−0.822	−0.470	−0.013
intercept_2	1.379	0.930	−0.910	−0.502	−0.777	−0.476	−0.082
slope_1	0.969	1.041	1.000	0.978	1.031	1.007	0.994
slope_2	0.961	1.002	1.037	0.997	1.049	1.016	1.004
SEE_1	0.884	1.036	0.331	0.263	0.604	0.656	0.170
SEE_2	1.103	1.264	0.329	0.254	0.560	0.606	0.174

TABLE III. Root mean square (rms), mean, and standard deviations of depth errors in mm (values for observer 1 are indicated by subscript 1, and for observer 2 by subscript 2).

	3°	3° zoom	6°	6° zoom	3° mag	3° mag zoom	6° mag
RMS_1	0.963	1.077	0.820	0.550	0.839	0.766	0.179
RMS_2	1.520	1.553	0.706	0.582	0.702	0.692	0.179
Mean $error_1$	0.420	0.354	−0.754	−0.482	−0.591	−0.421	−0.064
Mean $error_2$	1.068	0.945	−0.619	−0.527	−0.417	−0.357	−0.053
Std dev_1	0.877	1.030	0.326	0.268	0.603	0.648	0.169
Std dev_2	1.095	1.247	0.343	0.251	0.571	0.600	0.173

The computed rms errors (relative to the true depths) for the two independent readings were essentially identical (0.706 mm).

IV. DISCUSSION

The average rms errors for the two observers reading the same sets of images (Table III) were 1.2 mm (±3° contact, no zoom), 1.3 mm (±3° contact, zoom), 0.8 mm (±6° contact, no zoom), 0.6 mm (±6° contact, zoom), 0.8 mm (±3° magnification, no zoom), 0.7 mm (±3° magnification, zoom), and 0.2 mm (±6° magnification, no zoom). Corresponding values for the one observer who viewed all images of the phantom in three different layer configurations (Tables III and IV) were 1.6, 1.5, 0.7, 0.7, 0.5, 0.6, and 0.2 mm, respectively. In general, better results were obtained for the larger shift angle and for magnification geometry. Both of these improvements are in agreement with the analysis by Jiang *et al.* of the theoretical trends for stereo localization accuracy.[17] According to Jiang *et al.*, depth (z) localization error is inversely proportional to the x-ray tube shift (which is approximately equal to the tangent of the shift angle in our case), and directly proportional to the square of the focal spot-to-object distance (i.e., the error is smaller when the object is closer to the focal spot as in magnification geometry). Jiang *et al.* also showed that the sensitivity of the measurements to small changes in depth is proportional to the tube shift, and inversely proportional to the square of the focus-to-object distance.

Combining both observers' experimental results for all contact geometry images, we found that increasing the stereo shift angle from the conventional ±3° to ±6° improved the depth measurement accuracy by factors of about 1.2 to 4.0. The theoretical improvement considering only geometric factors[17] is approximately equal to the ratio of the tangents of the stereo shift angles which is 2.0 for this case (=tan 6°/tan 3°).

The variability in our results may be due to other sources of error. These include errors in the x-ray tube and slider positions for the acquisition of both the test phantom and calibration step wedge images, errors in the matching of the fiducial marker positions in the images for the desired 0 displacement at the bottom of the phantom, errors due to the limitation of a minimum 1 pixel (as opposed to fractional pixel) increment in the positioning of the virtual cursor for the z-value measurements in the test phantom and calibration phantom images, and uncertainties in the readers' determination of the cursor depth to overlay the fibril. The error in the measured depth due to the 1-pixel increment in the virtual cursor position is a function of the imaging geometry and can be computed by taking the derivative of the slope of the calibration line (Table I). This error is 1.18 mm for the ±3° stereo shift-contact geometry and 0.60 mm for the ±6° stereo shift-contact geometry. Thus, a change of 1 z-value unit in an observer's depth measurement of a fibril has a much greater effect for ±3° contact than for 6° contact geometry.

Comparing all measurements in the magnification versus contact geometries, we found improvements in depth accuracy by factors of 1.1–10.2 for ±3° magnification versus ±3° contact and by factors of 3.0–4.6 for ±6° magnification versus ±6° contact. The theoretical improvement due to geometrical factors in both cases is approximately proportional to the square of the ratio of the focus-to-object distances.[17] Considering a fibril located at about the midplane of the phantom (5 mm from the bottom of the phantom), and using the actual focus-to-magnification stand distance of 39.6 cm, and the focus-to-detector distance of 66 cm (assuming, for simplicity, that in the contact mode, the phantom is directly

TABLE IV. Root mean square (rms), mean, and standard deviations of depth errors in mm for two additional images read by observer 2.

	3°	3° zoom	6°	6° zoom	3° mag	3° mag zoom	6° mag
$RMS_{image\ 2}$	0.813	0.572	0.632	0.782	0.641	0.763	0.174
$RMS_{image\ 3}$	2.483	2.422	0.624	0.854	0.244	0.233	0.189
Mean $error_{image\ 2}$	0.691	0.303	0.373	0.620	−0.218	−0.271	0.031
Mean $error_{image\ 3}$	2.239	2.045	0.567	0.829	0.057	0.027	0.086
Standard $dev_{image\ 2}$	0.433	0.490	0.515	0.482	0.610	0.722	0.174
Standard $dev_{image\ 3}$	1.086	1.314	0.263	0.208	0.240	0.234	0.170

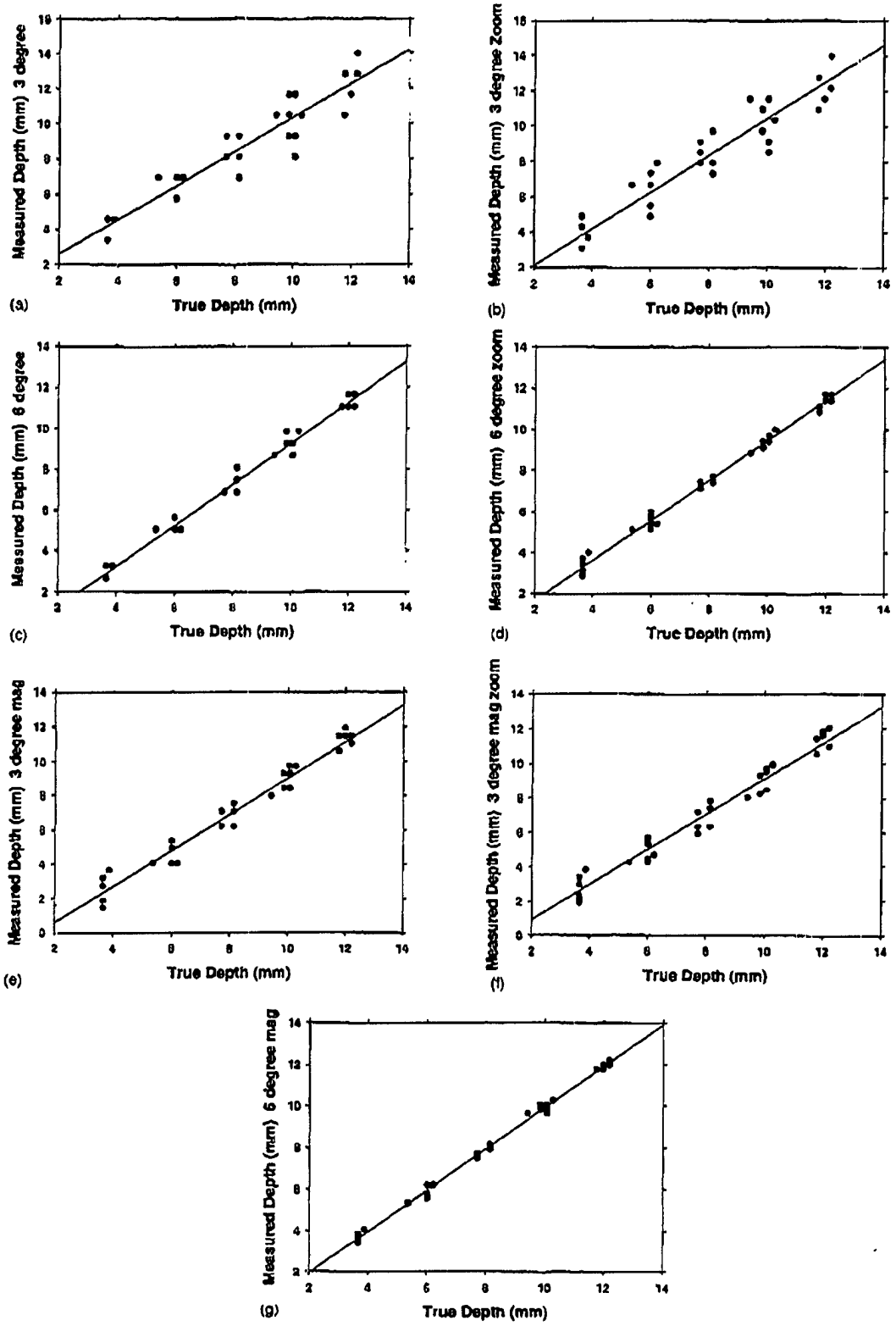

FIG. 4. Examples of measured versus true depths (distances from the back of the phantom) for observer number 1. (a) Stereo shift angle = ±3°, contact, no zoom; (b) stereo shift angle = ±3°, contact, zoom=2; (c) stereo shift angle = ±6°, contact, no zoom; (d) stereo shift angle = ±6°, contact, zoom=2; (e) stereo shift angle = ±3°, magnification mode, no zoom; (f) stereo shift angle = ±3°, magnification mode, zoom=2; (g) stereo shift angle = ±6°, magnification mode, no zoom.

TABLE V. p values for the paired t tests comparing the differences between the observed and measured z coordinates of the fibrils for the various stereoscopic imaging and display techniques (values are for three phantom configurations (different fibril patterns) analyzed by observer 2 (*=not significant since $p>0.05$; the rest are significant; *note:* the value of 0.000 00 means $p<10^{-5}$).

A Phantom layer configuration #1

	3° contact zoom	6° contact	6° contact zoom	3° mag	3° mag zoom	6° mag
3° contact	0.22191*a	0.00000	0.00000	0.00000	0.00000	0.00000
3° contact zoom		0.00000	0.00000	0.00002	0.00005	0.00001
6° contact			0.04878	0.03859a	0.01282	0.00000
6° contact zoom				0.27275*a	0.10784*a	0.00000
3° mag					0.03496	0.00039
3° mag zoom						0.00416

a indicates not significant ($p>0.05$) for observer 1

B. Phantom layer configuration #2

	3° contact zoom	6° contact	6° contact zoom	3° mag	3° mag zoom	6° mag
3° contact	0.00000	0.00123	0.46220*	0.00000	0.00000	0.00000
3° contact zoom		0.27320*	0.00008	0.00046	0.00066	0.00152
6° contact			0.00000	0.00031	0.00045	0.00012
6° contact zoom				0.00000	0.00000	0.00000
3° mag					1.14830*	0.00541
3° mag zoom						0.00538

C. Phantom layer configuration #3

	3° contact zoom	6° contact	6° contact zoom	3° mag	3° mag zoom	6° mag
3° contact	0.01394	0.00000	0.00000	0.00000	0.00000	0.00000
3° contact zoom		0.00000	0.00000	0.00000	0.00000	0.00000
6° contact			0.00000	0.00000	0.00000	0.00000
6° contact zoom				0.00000	0.00000	0.00000
3° mag					0.25839*	0.45679*
3° mag zoom						0.11153*

on top of the detector, and the fulcrum is in the plane of the detector), the theoretical improvement in depth accuracy is about a factor of 2.8. Variations in the observed improvements can be attributed to the reasons listed above.

In three of four cases, the measurement accuracies for ±3° magnification geometry were nearly identical to those for ±6° contact geometry. In one case, the accuracy was significantly superior (0.24 mm vs 0.62 mm) in ±3 magnification as compared to ±6° contact. The theoretical improvements due to geometrical considerations for this comparison is about 1.4. (As discussed above, the ±6° contact results should be better than the ±3° contact by a factor of 2 due to the increased tube shift, and the ±3° magnification results should be better than the ±3° contact by a factor of 2.8 due to the reduced focus-to-object distance. Combining these factors, the ±3° magnification measurements should be more accurate than ±6° contact by a factor of 1.4 (=2.8/2). The errors due to one-unit variations in the measured z values for the two geometries are similar (0.6 mm for ±6° contact and 0.42 mm for ±3° magnification.) Considering these factors and the other sources of measurement error discussed previously, the lack of observed improvement for the ±3° magnification geometry as compared to the ±6° contact geometry in most cases is not surprising. It should be noted that the rms errors for both geometries are very small (less than 1 mm) so either geometry would be adequate for making depth measurements.

Zooming the stereo images by a factor of 2 did not seem to improve the depth measurement accuracy. Although sometimes it appeared to improve the accuracy (7 of 12 times), other times it reduced the accuracy (5 of 12 times). There was basically no improvement on average (the difference in the average rms error for no zoom versus zoom, was 0.14 mm). The small differences one way or the other were there-

fore likely caused by experimental uncertainties due to the many factors described above. Thus, artificially increasing the displacement between objects viewed in the left- and right-eye stereo pairs through zooming the display does not have the same effect as increasing the displacement via increasing the stereo shift angle or increasing the geometric magnification. The stereo effect was more readily visualized in the zoom mode, but the signal-to-noise ratios of the fibril images were basically the same as those in the images displayed without zoom. In contrast, the acquisition of images with geometric magnification actually improves the signal-to-noise ratio.[18] The 2× zoom that was employed in this study was achieved by pixel replication. Results may be different for interpolative zoom. Finally, the use of greater zoom factors was also not explored. However, based on the results of a recently published study, increasing the display zoom factor may not be beneficial.[19] In that study, the observers' stereoacuities and depth perceptions were compared using a standard Randot stereotest pattern, with and without magnification via a 4× optical loupe and a 16× microscope. The researchers found that stereo acuity and depth perception decreased with increasing optical magnification of the pattern.

The paired *t*-test results listed in Table V indicate the majority of the differences between the depth measurement accuracies obtained with the ±3° and ±6° stereo shift angles, magnification and contact geometries, and normal and zoom displays are statistically significant ($p<0.05$). It is interesting to note that there was little consistency between the categories of the small number of insignificant differences ($p>0.05$) for the images created with the three different phantom configurations (parts A, B, and C of Table V). The only consistent insignificant result was that in two of the three cases, the accuracies for the ±3° mag and ±3° mag zoom depth measurements were not statistically significant. The *t*-test results for the two observers were quite similar for phantom configuration #1 (see footnote "a" of Table V, part A). Increasing the number of observers would have increased the statistical power of this study; however, the variability in the results due to the various factors described above would not have been reduced. Therefore the conclusions would likely be the same.

The best accuracy of about 0.2 mm, among all cases, was obtained with geometric magnification using a stereo angle of ±6°. Therefore, this is the mode we recommend for obtaining accurate depth measurements with virtual cursors in stereomammograms. Conventional stereoradiography is performed in contact mode using a stereo shift angle of ±3°. According to Christensen,[20] this angle was determined empirically "by trial and error." The angle is a compromise between the improved stereoscopic effect with increasing angle, the increased eye strain and difficulty in fusing the left- and right-eye images, especially at larger stereo angles, and the reduced patient coverage at larger stereo angles. For our particular case, the increased stereoscopic effect associated with the use of twice the conventional stereo angle and the use of ~1.8× geometric magnification did not cause undue eye strain. It did reduce the imaged field of view and this geometry could not be used for imaging an entire breast unless a larger-area detector was employed. Based on our measurements and observations, we recommend for stereoscopic imaging and depth measurements within an entire breast with the GE full-field digital mammography system, that a contact geometry be employed using a stereoshift angle of ±6° instead of the conventional ±3°. The overall results and recommendations of this study may differ for detectors having different pixel sizes and noise properties and for displays with different noise and contrast. A further investigation of the effects of these factors is warranted.

Finally, the depth measurement accuracies of the two observers in this study (Table III) were almost identical (in nearly all cases they were within 0.1 mm of each other). Both observers had excellent stereo acuity, and it would be expected that others with similar stereo acuity could achieve similar results after a period of training. Our previous studies with other observers have shown that there is a wide range of accuracies for depth measurements, especially for horizontally oriented objects.[3] All of the fibrils in this study had horizontal and vertical components, so it would be expected that even observers who have difficulties measuring the depths of horizontally oriented objects would be able to measure the depths of the diagonally oriented fibrils, although their accuracies may not be as high. Since it is unlikely that fibrous tissues or spicules from masses in mammograms are exactly horizontal to the stereo shift direction, the angulation would enable reasonably accurate measurements in clinical images. However, the inhomogeneous anatomical background within the clinical images may partially obscure the fibrils, which would increase the difficulty of making accurate depth measurements with the stereo cursor. It is possible that with additional training and the use of depth cues (e.g., 3-D wire boxes placed about the objects of interest, or 3-D rulers in the image) in clinical images, the depth measurement accuracies of most viewers would be adequate. The development of such depth cues will be the subject of our future investigations.

ACKNOWLEDGMENTS

This work is supported by U.S. Army Medical Research and Material Command Grants No. DAMD 17-98-1-8210 and No. DAMD 17-99-1-9294. The content of this publication does not necessarily reflect the position of the funding agency, and no official endorsement of any equipment and product of any companies mentioned in this publication should be inferred.

[a]Corresponding author: Department of Radiology, University of Michigan Hospitals, Room B1 F510C, 1500 East Medical Center Drive, Ann Arbor, Michigan 48109-0030. Office 734-936-7474; Fax: 734-936-7948; Electronic mail: goodsitt@umich.edu

[1]D. M. Chelberg, J. Hsu, C. G. Babbs, Z. Pizlo, and E. J. Delp, "Digital stereomammography," in *Proceedings of the 2nd International Workshop on Digital Mammography*, Excepta Medica International Congress Series 1069 (Elsevier Science, York, England, 1994), pp. 181–190.

[2]J. Hsu, D. M. Chelberg, C. F. Babbs, Z. Pizlo, and E. J. Delp, "Preclinical ROC studies of digital stereomammography," IEEE Trans. Med. Imaging 14, 318–327 (1995).

[3] M. M. Goodsitt, H.P. Chan, and L. M. Hadjiiski, "Stereomammography: Evaluation of depth perception using a virtual 3D cursor," Med. Phys. 27, 1305–1310 (2000).
[4] D. J. Getty, R. M. Pickett, and D. J. D'Orsi, "Stereoscopic digital mammography: improving detection and diagnosis of breast cancer," in *Computer Assisted Radiology and Surgery 2001*, Proceedings of the 15th International Congress and Exhibition, Berlin, 27–30 June 2001, edited by H. U. Lemke, M. W. Vannier, K. Inamura, A. G. Farman, and D. Doi (Elsevier, Amsterdam, 2001; International Congress Series 1230), pp. 506–511.
[5] M. M. Goodsitt, H. P. Chan, J. M. Sullivan, K. L. Darner, and L. M. Hadjiiski, "Evaluation of the effect of virtual cursor shape on depth measurements in digital stereomammograms," in *IWDM 2000 5th International Workshop on Digital Mammography*, edited by M. J. Yaffe (Medical Physics Publishing, Madison, 2001), pp. 45–50.
[6] H. P. Chan, M. M. Goodsitt, K. L. Darner, J. M. Sullivan, L. M. Hadjiiski, N. Petrick, and B. Sahiner, "Effects of stereoscopic imaging technique on depth discrimination," in Ref. 5, p. 13–18.
[7] B. Leduc, R. Shumak, G. E. Mawdsley, M. J. Yaffe, and R. A. Jong, "Merits of using a 3-D visualization technique to target microcalcifications," in Ref. 5, pp. 56–64.
[8] L. T. Niklason *et al.*, "Digital tomosynthesis in breast imaging," Radiology 205, 399–406 (1997).
[9] R. L. Webber, H R. Underhill, and R. I. Freimanis, "A controlled evaluation of tuned-aperture computed tomography applied to digital spot mammography," J. Digit. Imaging 13, 90–97 (2000).
[10] S. Suryanarayanan, A. Karellas, S. Vedantham, S. P. Baker, S. J. Glick, C. J. D'Orsi, and R. L. Webber, "Evaluation of linear and nonlinear tomosynthetic reconstruction methods in digital mammography," Acad. Radiol. 8, 291–224 (2001).
[11] V. Raptopoulos, J. K. Baum, M. Hochman, A. Karellas, M. J. Houlihan, and C. J. D'Orsi, "High resolution CT mammography of surgical biopsy specimens," J. Comput. Assist. Tomogr. 20, 179–184 (1996).
[12] J. M. Boone, T. R. Nelson, K. K. Lindfors, and J. A. Seibert, "Dedicated breast CT: Radiation dose and image quality evaluation," Radiology 221, 657–667 (2001).
[13] S. L. Warren, "Roentgenologic study of the breast," Am. J. Roentgenol. 24, 113–124 (1930).
[14] A. D. A. Maidment, P. Bakic, and M. Albert, "Is stereomammography possible without increasing dose?," *The 6th International Workshop on Digital Mammography*, 22–25 June 2002, Bremen, Germany, Program & Abstracts, 2002, p. 27.
[15] S. Vedantham, A. Karellas, S. Suryanarayanan, D. Albagli, S. Han, E. J. Tkaczyk, C. E. Landberg, B. Opsahl-Ong, P. R. Granfors, I. Levis, C. J. D'Orsi, and R. E. Hendrick, "Full breast digital mammography with an amorphous silicon-based flat-panel detector: physical characteristics of a clinical prototype," Med. Phys. 27, 558–567 (2000).
[16] K. Simons, "Stereoacuity norms in young children," Arch. Opthalmol. 99, 439–445 (1981).
[17] H. Jiang, H. Liu, G. Wang, W. Chen, and L. L. Fajardo, "A localization algorithm and error analysis for stereo x-ray image guidance," Med. Phys. 27, 885–893 (2000).
[18] K. Doi and H. Imhof, "Noise reduction by radiographic magnification," Radiology 122, 479–487 (1977).
[19] L. T. Du, L. F. Wessels, J. P. Underdahl, and J. D. Auran, "Stereoacuity and depth perception decrease with increased instrument magnification: comparing non-magnified system with lens loupes and a surgical microscope," Binocul. Vis. Strabismus. Q. 16, 61–67 (2001).
[20] T. S. Curry, J. E. Dowdey, and R. C. Murry, *Christensen's Physics of Diagnostic Radiology*, 4th ed. (Lea & Febiger, Philadelphia, 1990).

Digital Stereomammography: Observer Performance Study of the Effects of Magnification and Zooming on Depth Perception

Heang-Ping Chan, Mitchell M. Goodsitt, Lubomir M. Hadjiiski, Janet E. Bailey, Katherine Klein, Katie L. Darner, Chintana Paramagul

Department of Radiology, University of Michigan, Ann Arbor, MI 48109

ABSTRACT

We have previously reported the effects of stereo angle and exposure on depth discrimination and the use of virtual cursors for absolute depth measurements in digital stereomammography. The current study further investigates the effects of magnification and zooming on depth perception. Stereoscopic image pairs of a phantom were acquired with a full-field digital mammography system. The modular phantom contained 25 crossing fibril pairs with depth separations between each pair ranging from 2 to 10 mm. Three phantom (fibril) configurations were imaged using techniques of 30 kVp, Rh/Rh, ±3° stereo angle, , contact and 1.8X magnification geometry, and 4 to 63 mAs exposure range . The images were displayed on a Barco monitor driven by a Metheus stereo graphics board and viewed with LCD stereo glasses. Five observers participated in the study. Each observer visually judged if the vertical fibril was in front of or behind the horizontal fibril in each pair. It was found that the accuracy of depth discrimination increased with increasing fibril depth separation and x-ray exposure. Zooming the contact stereo images by 2X did not improve the accuracy. Under conditions of high noise (low mAs) and small depth separation between the fibrils, depth discriminations were significantly better in stereo images acquired with geometric magnification than in images acquired with a contact technique and displayed with or without zooming. This study indicates that stereoscopic imaging, especially with magnification, may be useful for visualizing the spatial distribution of microcalcifications in a cluster and differentiating overlapping tissues from masses on mammograms.

KEY WORDS: Digital mammography, stereoscopic imaging, magnification, observer performance study.

1. INTRODUCTION

Mammography is the most sensitive method for detecting early breast cancers. However, because of the projection of the breast tissues along the x-ray beam path onto a two-dimensional image plane, one of the major limitations in mammography is the low sensitivity for detecting lesions overlapping with dense fibroglandular tissues[1]. It has been estimated that about 20% of breast cancers in dense breasts are missed [2, 3]. The camouflaging effect of overlapping structures is the main cause of missed diagnoses. New breast imaging techniques such as stereomammography[4-7], digital tomosynthesis[8, 9], and computed tomography[10] may alleviate this problem.

Stereoscopic imaging requires acquisition of two images. The x-ray focal spot is shifted, along a direction parallel to the image plane, to the left and the right of the central axis to obtain two images, referred to as the left-eye and the right-eye images, respectively, of the object. When the two images are placed properly and viewed so that the left eye sees only the left-eye image and the right eye sees only the right-eye image, the parallax between the two images creates the depth perception. Stereoscopic radiography has been attempted for different types of examinations but it has not achieved widespread acceptance in clinical practice, however, mainly because of the doubled film cost and increased patient exposure [11]. The recent advent of direct digital detectors may make the stereoscopic technique a viable approach because no additional film cost will be required. Furthermore, a digital detector has a wider dynamic range and higher contrast sensitivity than a screen-film system so that good-quality images may be acquired at a reduced radiation dose. Digital stereoscopic images can be viewed on a single display monitor with the assistance of stereoscopic goggles that provide an electronic shutter to show the left- and right-eye images to the respective eyes. The stereoscopic images can therefore be displayed singly in the conventional manner or stereoscopically on the same viewing station to provide complementary diagnostic information.

An advantage of stereoscopic imaging is the three-dimensional (3D) structural information that it provides for the lesions of interest. The 3D distribution of microcalcifications may be correlated with the malignant or benign nature of the cluster[12, 13]. Spiculations from a mass may also be more readily distinguished from overlapping tissues under stereoscopic

Medical Imaging 2002: Physics of Medical Imaging, Larry E. Antonuk, Martin J. Yaffe, Editors,
Proceedings of SPIE Vol. 4682 (2002) ©2002 SPIE-1605-7422/02/$15.00

viewing conditions. The additional diagnostic information may improve the classification of malignant and benign lesions, thereby reducing unnecessary biopsies. It has been reported that digital stereomammography allowed the detection of additional lesions that were obscured on screen-film mammograms[4].

We are investigating the usefulness of stereomammography for discriminating the depths of subtle mammographic features. We previously demonstrated that a virtual cursor could provide accurate depth measurements in stereo phantom images acquired under mammographic conditions[5, 6, 14]. We also studied the effects of stereo shift and imaging conditions on the depth perception of crossing fibrils in stereo phantom images[15]. In this study, we further evaluated the effects of geometric magnification, display zooming, and x-ray exposure on the visual depth discrimination of fibril-like objects in stereo phantom mammograms. The results of our observer performance study are discussed in this paper.

2. MATERIALS AND METHODS

2.1 Phantom Design

We have designed a modular stereo phantom for evaluation of the depth perception task. The phantom consists of six 1-mm-thick Lexan sheets, each separated by 1-mm-thick spacers. Each Lexan plate contains a 5 X 5 array of object areas. Fifty nylon fibrils, each about 8-mm in length and 0.53 mm in diameter, are arranged in these object areas. Twenty-five fibrils are oriented vertically (perpendicular) and 25 horizontally (parallel) to the stereo shift direction. The fibrils are placed in the object areas on the six Lexan plates such that, in the projection image, each object area contains the projection of one vertical and one horizontal fibril that cross each other. The depth separation of each pair of crossing fibrils depends on the arrangement of the plates. These plates can be arranged in different orders to produce many independent object configurations.

2.2 Image Acquisition and Display

Digital stereoscopic image pairs were acquired with a GE Senographe 2000D digital mammography system. The system employs a digital detector consisting of a CsI:Tl scintillator and an amorphous-Si active matrix flat panel. The detector measures 23 cm x 18 cm, with a pixel size of 100 μm x 100 μm. We acquired stereoscopic pairs of images using x-ray techniques of 30 kVp, Rh target/Rh filter, a ±3° stereo-angle, contact (reciprocating grid, 0.3 mm focal spot) and 1.8X magnification (no grid, 0.15 mm focal spot) geometies, and exposures of 4, 8, 32, and 63 mAs per image. Three different configurations of the fibril phantoms were imaged under each exposure condition. Twenty-four stereo image pairs were thus produced. For each exposure/geometry condition, there were a total of 75 pairs of fibril images (25 fibril pairs in each phantom configuration x 3 configurations) at 5 different depth separations (2, 4, 6, 8, 10 mm) to be evaluated.

The images were displayed on a 21" Barco-Metheus (Beaverton, OR) model 521 display monitor driven by a model 1760S stereoscopic board and a SUN Microsystems (Palo Alto, CA) Ultra 10 computer. The Metheus board displays 1408 x 1408 x 8 bit images at a refresh rate of 114 Hz . It operates in a page flipping stereoscopic mode with the left- and right-eye images displayed alternately. NuVision (Beaverton, OR) LCD stereoscopic glasses were used for viewing the stereoscopic images.

2.3 Observer Experiment

Five observers including two experienced mammographic radiologists participated in the experiment. The contact images were read in two modes – a regular and a 2X-zoom mode. The 1.8X geometric magnification images were read only in the regular mode. The observers were asked to visually judge if the vertical fibril in each pair of overlapping fibrils was in front of or behind the horizontal fibril. Each observer read the images sequentially in a different randomized order. The observers were not informed of the conditions under which the image being viewed was acquired. Prior to reading the test cases, the observers participated in training sessions to become familiar with the reading task.

3. RESULTS

Tables 1-3 summarize the percentages of correct decisions on the relative depths as a function of the depth separation of the crossing fibrils, averaged over 5 observers, for the different exposure levels studied. The statistical

significance (two-tailed p level<0.05) of the differences between every two conditions: contact and contact-zoom, contact and magnification, and contact-zoom and magnification was estimated by a paired-t test. The t-test was performed for each depth separation and exposure level over the 5 observers. It was found that the differences between the contact and contact-zoom viewing conditions were not statistically significant. The differences between the contact and magnification geometries were statistically significant for depth separations of 2 mm to 6 mm at 4 mAs, and for 2-mm separation at 8 mAs. The differences between the contact-zoom and magnification were statistically significant for depth separations of 2 mm to 6 mm at 4 mAs, for 2-mm to 4-mm separations at 8 mAs, and for 2-mm separation at 32 mAs.

Table 1. The average percentage of correct decision in differentiating the depths of two crossing fibrils in stereo images acquired with contact geometry and displayed without zooming.

Depth Separation (mm)	Exposure			
	4 mAs	8 mAs	32 mAs	64 mAs
2	68.8	77.6	87.2	92.0
4	76.7	94.4	97.8	96.7
6	90.0	98.3	100.0	100.0
8	95.3	98.8	97.6	100.0
10	100.0	100.0	100.0	100.0

Table 2. The average percentage of correct decision in differentiating the depths of two crossing fibrils in stereo images acquired with contact geometry and displayed with 2X zoom.

Depth Separation (mm)	Exposure			
	4 mAs	8 mAs	32 mAs	64 mAs
2	72.8	83.2	89.6	93.6
4	81.1	91.1	98.9	100.0
6	83.3	98.3	100.0	100.0
8	91.8	96.5	96.5	100.0
10	100.0	100.0	100.0	100.0

Table 3. The average percentage of correct decision in differentiating the depths of two crossing fibrils in stereo images acquired with 1.8X magnification geometry and displayed without zooming.

Depth Separation (mm)	Exposure			
	4 mAs	8 mAs	32 mAs	64 mAs
2	92.0	93.6	97.6	98.4
4	98.9	100.0	100.0	100.0
6	98.3	100.0	100.0	100.0
8	100.0	98.8	100.0	100.0
10	100.0	100.0	100.0	100.0

4. CONCLUSIONS

This study shows that the accuracy of depth discrimination of fibrils in stereomammography increases with x-ray exposure and depth separation and depends on imaging geometry. Depth discrimination at ±3° stereo angle was reasonably good, 2-mm depth resolution was achieved with over 60% accuracy for all imaging conditions studied. It improved to greater than 90% accuracy at higher doses and contact geometry. Under our experimental conditions, zooming the contact stereo images by 2X did not improve the accuracy. When the images were noisy and the depth separation between the fibrils was small, depth discriminations were significantly better in stereo images acquired with geometric magnification than in images acquired with a contact technique and displayed with or without zooming. Magnification stereomammography

provided over 90% accuracy at 2-mm depth resolution for all exposure levels studied. These results indicate that stereoscopic imaging, and in particular, magnification stereomammography, may be useful for visualizing the spatial distribution of microcalcifications in a cluster and differentiating overlapping tissues from masses on mammograms. Further studies are underway to evaluate use of other stereo angles (e.g., ±6°) and to investigate if specially designed cursors can assist in depth discrimination and measurement of absolute depths of target objects in stereoscopic images[5, 6, 14].

ACKNOWLEDGMENTS

This work is supported by U. S. Army Medical Research and Materiel Command Grants DAMD 17-98-1-8210 and DAMD17-99-1-9294. The content of this publication does not necessarily reflect the position of the funding agency, and no official endorsement of any equipment and product of any companies mentioned in this publication should be inferred.

REFERENCES

1. V. P. Jackson, R. E. Hendrick, S. A. Feig and D. B. Kopans, "Imaging of the radiographically dense breast," Radiology 188, 297-301 (1993).
2. R. E. Bird, T. W. Wallace and B. C. Yankaskas, "Analysis of cancers missed at screening mammography," Radiology 184, 613-617 (1992).
3. M. G. Wallis, M. T. Walsh and J. R. Lee, "A review of false negative mammography in a symptomatic population," Clinical Radiology 44, 13-15 (1991).
4. D. J. Getty, R. M. Pickett and C. J. D'Orsi, "Stereoscopic digital mammography: improving detection and diagnosis of breast cancer," Computer Assisted Radiology and Surgery 2001, Proceedings of the 15th International Congress and Exhibition, Berlin, International Congress Series 1230, 506-511 (2001).
5. M. M. Goodsitt, H. P. Chan and L. M. Hadjiiski, "Stereomammography: Evaluation of depth perception using a virtual 3D cursor," Medical Physics 27, 1305-1310 (2000).
6. M. M. Goodsitt, H. P. Chan, J. M. Sullivan, K. L. Darner and L. M. Hadjiiski, "Evaluation of the effect of virtual cursor shape on depth measurements in digital stereomammograms," The 5th International Workshop on Digital Mammography, Toronto, Canada, Proc. IWDM-2000, 45-50 (2000).
7. H. P. Chan, M. M. Goodsitt, K. L. Darner, J. M. Sullivan, L. M. Hadjiiski, N. Petrick and B. Sahiner, "Effects of stereoscopic imaging technique on depth discrimination," The 5th International Workshop on Digital Mammography, Toronto, Canada, Proc. IWDM-2000, 13-18 (2000).
8. L. T. Niklason, B. T. Christian, L. E. Niklason, D. B. Kopans, D. E. Castleberry, B. H. Opsahl-Ong, C. E. Landberg, P. J. Slanetz et. al., "Digital tomosynthesis in breast imaging," Radiology 205, 399-406 (1997).
9. S. Suryanarayanan, A. Karellas, S. Vedantham, S. P. Baker, S. J. Glick, C. J. D'Orsi and R. L. Webber, "Evaluation of linear and nonlinear tomosynthetic reconstruction methods in digital mammography," Academic Radiology 8, 219-224 (2001).
10. J. M. Boone, T. R. Nelson and J. A. Seibert, "The potential for breast CT," Medical Physics 28, 1246 (abstract) (2001).
11. T. S. Curry, J. E. Dowdey and R. C. Murry, *Christensen's Physics of Diagnostic Radiology.*, Fourth ed. (Lea & Febiger, Philadelphia, PA, 1992).
12. A. D. A. Maidment, M. Albert, E. F. Conant, C. W. Piccoli and P. A. McCue, "Prototype workstation for 3-D diagnosis of breast calcifications," Radiology 201(P), 556 (1996).
13. E. F. Conant, A. D. Maidment, M. Albert, C. W. Piccoli, S. A. Nussbaum and P. A. McCue, "Small field-of-view digital imaging of breast calcifications: method to improve diagnostic specificity," Radiology 201(P), 369 (1996).
14. M. M. Goodsitt, H. P. Chan, K. L. Darner and L. M. Hadjiiski, "The effects of stereo shift angle, geometric magnification, and display zoom on depth measurements in digital stereomammography," Medical Physics (submitted) (2002).
15. H. P. Chan, M. M. Goodsitt, J. M. Sullivan, K. L. Darner and L. M. Hadjiiski, "Depth perception in digital stereoscopic mammography," Poster presentation at the Era of Hope Meeting, U. S. Army Medical Research and Materiel Command, Department of Defense, Breast Cancer Research Program, Atlanta, Georgia, (2000).

TU-C-517C-07

Automated Spot Mammography: A Comparison of Spot Imaging Regions Selected by Radiologists

M Goodsitt*, H-P Chan, C Gandra, N Chen, M Helvie, K Klein, J Bailey, C Paramagul, University of Michigan, Ann Arbor, MI

WE are developing an automated spot mammography technique for improved imaging of suspicious dense regions within digital mammograms. The ultimate implementation will entail automatic detection of regions for spot imaging, automatic collimation of the x-ray beam to those regions, and stereoscopic spot imaging and display. To gain a better understanding of the characteristics of regions that radiologists select for spot imaging, a graphical user interface was developed to allow radiologists to trace up to 3 spot imaging regions in a mammogram. An observer study was performed in which 4 MQSA-qualified mammographers traced regions in 177 digitized mammograms. Two of the radiologists performed the study twice to assess reproducibility. The BI-RADS density ratings of the images ranged from 2-4 (mean 2.6+/-0.6). The regions selected by radiologists were compared by computing ratios of the intersections to unions of the selected areas in each mammogram. The comparisons were performed for sets of 2 radiologists at a time. With 3 possible regions in each image for each radiologist there were 9 potential intersection to union ratios per image. The ratios were ordered from largest to smallest. Combining the results for all sets, the averages of the largest ratios ranged from 28%-46% (mean 37%+/-6%). The averages of the second largest ratios ranged from 6%-16% (mean 10%+/-3%). Corresponding values for the reproducibility studies were 43%-59% and 15%-27%. The agreement of the selected spot regions among radiologists will be discussed in detail. Images illustrating the comparisons and additional statistics will be presented.

DEVELOPMENT OF DIGITAL STEREO IMAGING TECHNIQUE FOR MAMMOGRAPHY

Heang-Ping Chan, Mitchell Goodsitt, Lubomir Hadjiiski, Mark Helvie, Janet Bailey, Katherine Klein, and Marilyn Roubidoux

Department of Radiology, University of Michigan, Ann Arbor, MI 48109

chanhp@umich.edu

One of the limitations of mammographic imaging is that overlapping dense tissue in the breast can camouflage true lesions or create false lesions in the projected image. The goal of this project is to develop a digital stereoscopic imaging technique for mammography. It is expected that overlying dense tissues will be separated from the lesion in the stereoscopic views, thereby increasing the conspicuity of the lesion, and that the ability to analyze the 3-dimensional (3D) distributions and shapes of lesions such as calcifications and masses can potentially improve the accuracy of mammographic interpretation by radiologists and reduce unnecessary biopsies.

We have investigated the dependence of depth discrimination on imaging parameters including the stereo angle, x-ray exposure, magnification, and display zoom. Image display software was developed for a high-quality stereo viewing station. Observer studies were conducted to view stereo images of 3D mammographic phantoms acquired under various imaging conditions. The accuracy of the observers in differentiating the relative depths of two overlapping fibrils was evaluated. In addition, we have developed 3D virtual cursors for measurement of the depth of objects in a stereomammogram. The effects of imaging parameters and virtual cursor shapes on depth measurement accuracy have been studied.

It was found that the accuracy of depth discrimination increased with increasing stereo angle, exposure, and fibril depth separation. Zooming the contact stereo images by 2X did not improve the accuracy. Under conditions of high noise and small depth separation between the fibrils, depth discrimination was significantly better in stereo images acquired with geometric magnification than in images acquired with a contact technique and displayed with or without zooming. Magnification mammography also provided the highest accuracy for depth measurement with a virtual cursor, whereas display zoom did not improve accuracy.

These studies indicate that stereoscopic imaging, especially with magnification, may be useful for differentiating overlapping tissues from masses on mammograms and visualizing the spatial distribution of microcalcifications in a cluster, thereby improving the accuracy of mammography for breast cancer detection and diagnosis.

Original work supported by the U.S. Army Medical Research and Materiel Command under DAMD17-98-1-8210.

AUTOMATED STEREO SPOT MAMMOGRAPHY FOR IMPROVED IMAGING OF DENSE BREASTS

Mitchell M. Goodsitt, Heang-Ping Chan, Chaitanya R. Gandra, Nelson G. Chen, and Mark A. Helvie

University of Michigan

goodsitt@umich.edu

One of the primary limitations of present day x-ray mammography screening is the poor detectability of cancers within dense breasts. Even the new digital mammography systems will not completely solve this problem. We are developing a novel automatic stereo spot technique for improved imaging with the digital mammography systems. The basic idea is to automatically detect any suspicious dense region within the full-field digital mammogram, and within seconds take a stereo digital mammogram of only that region using automated collimation, manual x-ray tube shift, and more penetrating exposures.

Software was developed to allow radiologists to trace suspicious dense regions within mammograms, and an observer study was performed to assess the agreement of the selected regions. Prototype devices were designed and built to automatically collimate the beam to the selected region and position a spot compression paddle at that region. Experiments were performed with breast-simulating phantoms to compare combined spot compression and collimation to spot collimation with stereoscopic image acquisition.

Ratios of the intersections to unions of the selected regions were computed for each set of 2 radiologists. Combining the results for all sets, the averages of the largest ratios ranged from 28%-46% (mean 37%+/-6%). The averages of the second largest ratios ranged from 6%-16% (mean 10%+/-3%). Corresponding values for the reproducibility of regions selected by individual radiologists were 43%-59% and 15%-27%. For the phantom study, an in-house developed 3-D virtual cursor was used to measure the separations between overlapping simulated masses in stereoscopic images obtained with and without spot compression. Spot compression was found to reduce the spacing between the masses. The improved visualization of overlapping tissues with stereoscopic imaging and reduced complexity in system design and operation caused us to favor and pursue developing stereo imaging with spot collimation.

It is anticipated that automated stereo spot mammography will significantly improve the detection and characterization of masses in dense breasts in routine screening and will therefore improve the accuracy of screening programs.

The U.S. Army Medical Research and Materiel Command under DAMD17-99-1-9294 supported this work.

subtraction imaging, where separate low- and high-energy images are acquired and synthesized to *cancel* the tissue structures, offers an alternative approach for visualizing μCs.

Transmission measurements at two different kVp were made on breast phantoms for different combinations of tissue thickness, tissue composition (glandular versus adipose), and aluminum (to mimic μC) thickness, under narrow beam geometry using an indirect flat-panel mammographic imager. In principle, two images could provide information on two unknowns. Three different scenarios with two unknowns were explored by varying: (1) tissue composition and tissue thickness; (2) Al thickness and tissue thickness (fixed composition); and (3) Al thickness and tissue composition (fixed thickness).

The measured transmission data were found to vary as 2nd-order polynomials for all three scenarios. The coefficients of the mapping functions (3rd-order polynomials) for material thickness/composition from dual-energy measurements were calculated by least-squares analysis. The uncertainties in the model prediction were estimated by comparing the model predictions with the known values. The (1σ) uncertainties in the model predictions are: (1) 0.8 mm for tissue thickness and 3.5% glandular for tissue composition; (2) 16 μm for Al thickness and 0.25 mm for tissue thickness; and (3) 48 μm for Al thickness and 5% glandular for tissue composition. The uncertainties quoted do not account for the noise in the raw images.

TU-C-517C-04

A Feasibility Study for CNR Based Technique Selection in Digital Mammography

N Bezrukiy*, V Cooper, UCLA School of Medicine, Los Angeles, CA

Digital mammography is gaining popularity due to decoupled acquisition and display that it offers, increased dynamic range, as well as the ease of image manipulation, handling and storage. Historically, the AEC logic on film-screen mammography systems was designed to keep the OD within a certain range, but with the addition of the new digital technologies, such as flat panel and computed radiography (CR), the logic needs to be reassessed. In this work we perform an experimental feasibility study to evaluate the usefulness of contrast-to-noise ratio (CNR) as a criterion for technique selection in digital mammography. The CNR measurements were performed on the both flat panel and CR units for a 4.5 cm (50% fat – 50% glandular) breast phantom. Evaluation of CNR as a function of exposure and mean glandular dose (MGD) was performed for a range of anode/filter/kVp combinations in order to determine the optimal technique. The theoretical square root relationship between exposure and CNR, as well as between CNR and MGD were confirmed by the experiments. For a 250 mrad MGD limit (Mo/Mo, 25 kVp, 0.354 mm Al) the images obtained with the flat panel detector produced the highest CNR value of 3.73. This proof of principle study warrants further investigation into the methodology, which will follow.

TU-C-517C-05

Clinical X-Ray Exposure Comparison of Film-Screen and Flat Panel Detection Systems in Mammography: ACR Phantom Imaging

V Cooper*[1], T Oshiro[1], C Cagnon[1], L Bassett[1], T McLeod[2], (1) UCLA Medical Center, Los Angeles, CA, (2) University of Michigan, Ann Arbor, MI

Digital detectors in mammography have wider dynamic range than film-screen systems, but the quantification of that width in the clinical exposure domain is unclear. In this work, we compare the range of mAs values, and hence, exposure values, that may be used to produce acceptable ACR phantom images with flat panel and screen-film systems (independent of dose constraints). The range of acceptable mAs values for the contrast-limited film-screen system was defined as that ratio of mAs values for a 26 kVp Mo/Mo (HVL=0.34 mm Al) beam that yielded passing scores for fibers, speck groups, and masses. The range of acceptable mAs values for the noise-limited digital system was defined as the ratio of mAs values over which the ACR phantom images were acceptable and the pixel statistics followed the expected relationship with exposure (i.e., quantum-limited). Three independent observers and 30 observations each indicated that the film-screen system had an acceptable mAs-ratio range of 2.2 ± 0.53 (200/90). Across all observers, the detection of the third speck group was the limiting factor. With windowing, leveling, and magnification of the raw linear data, the third speck group could be visualized down to 20 mAs for the digital system, but the quantum-limited end-point corresponded to 40 mAs. The 40 mAs quantum-limited endpoint was also confirmed for the log-processed data. No saturation within the imaged phantom was achieved even at 400 mAs. Thus, the digital system yielded at least 4.5 times greater latitude in imaging the ACR phantom.

TU-C-517C-06

Digital Vs. Film-Screen Mammography: Radiation Dose and SNR

E Nickoloff*[1], A Dutta[1], Z Lu[1], S Smith[1], R Rosenblatt[2], (1)New York-Presbyterian Hospital & Columbia University, New York, NY, (2)Cornell Medical Center, New York, NY

The purpose of this study was to compare the performance of two different full-field, digital mammography units to their corresponding film-screen units. The average glandular dose and the signal-to-noise ratio (SNR) were determined for a range of phantom thickness.

The GE Senographe 2000-D digital mammography unit was compared to a GE DMR Plus film-screen unit. A Lorad Contour 2000 CCD unit was compared to a Lorad M-IV Platinum film-screen unit. These data were also compared to the GE units. Plastic BR-12, which simulates 50% adipose breast tissue, was used to measure the typical radiation levels for the dose calculations. Uniform acrylic sheets were used to measure SNR for various radiation dose levels.

Dependent upon the selection of exposure parameters, the digital units delivered similar average glandular doses to the film-screen units. However, in certain modes, the radiation levels were lower due to the utilization of higher kVp's, filtration and other factors. For the digital systems, the SNR increases with the square root of the mAs. The dynamic range of digital systems is greater than film-screen units, which influences the low contrast visualizations. Each imaging modality has certain inherent advantages and disadvantages. Film-screen systems have better spatial resolution. Digital mammography has wider dynamic range and variable displays. It is important to note that low contrast visualization for digital systems is closely tied to SNR and display features, which can be important in clinical applications.

TU-C-517C-07

Automated Spot Mammography: A Comparison of Spot Imaging Regions Selected by Radiologists

M Goodsitt*, H-P Chan, C Gandra, N Chen, M Helvie, K Klein, J Bailey, C Paramagul, University of Michigan, Ann Arbor, MI

WE are developing an automated spot mammography technique for improved imaging of suspicious dense regions within digital mammograms. The ultimate implementation will entail automatic detection of regions for spot imaging, automatic collimation of the x-ray beam to those regions, and stereoscopic spot imaging and display. To gain a better understanding of the characteristics of regions that radiologists select for spot imaging, a graphical user interface was developed to allow radiologists to trace up to 3 spot imaging regions in a mammogram. An observer study was performed in which 4 MQSA-qualified mammographers traced regions in 177 digitized mammograms. Two of the radiologists performed the study twice to assess reproducibility. The BI-RADS density ratings of the images ranged from 2-4 (mean 2.6+/-0.6). The regions selected by radiologists were compared by computing ratios of the intersections to unions of the selected areas in each mammogram. The comparisons were performed for sets of 2 radiologists at a time. With 3 possible regions in each image for each radiologist there were 9 potential intersection to union ratios per image. The ratios were ordered from largest to smallest. Combining the results for all sets, the averages of the largest ratios ranged from 28%-46% (mean 37%+/-6%). The averages of the second largest ratios ranged from 6%-16% (mean 10%+/-3%). Corresponding values for the reproducibility studies were 43%-59% and 15%-27%. The agreement of the selected spot regions among radiologists will be discussed in detail. Images illustrating the comparisons and additional statistics will be presented.